

Comments from Referee #1

1 General comments

Zhang et al. investigate in their manuscript the effect of relative humidity on the aerosol light scattering for a rural site in the Yangtze River Delta in China. The results of a one-month campaign are presented, which includes measurements of the scattering enhancement factor $f(RH)$, the particle chemical composition and absorption properties in addition to standard meteorological parameters. The relative contribution of inorganic to organic mass fraction was found to be the main parameter determining the magnitude of the scattering enhancement. The results were further analyzed using a trajectory analysis and estimating the effect on the direct radiative forcing.

*The findings are of general interest to the scientific community since only few measurements of $f(RH)$ exist from that region of the world. The manuscript is plausibly structured and the results are presented in an appropriate way. However, there is still room for improvement by clarifying specific comments, by removing some redundancies, and by additional editorial work (spelling and grammar mistakes). Currently, some needed instrumental and calibration details are missing in the manuscript. An optical closure study using Mie theory would help to put the measurements on a more trustworthy basis. Overall, I recommend the paper to be published in ACP after the following comments have been answered satisfactorily (**major revisions**).*

Thanks for reviewer's suggestions. We have revised the manuscript accordingly. The following are our responses:

2 Specific comments (in arbitrary order)

1. Sect. 2.2 (Measurement system):

(1) Please state the mean and STD of the RH inside the DryNeph. There are also some inconsistencies within the text concerning the RH which has been regarded as dry (30% or 40%?), please precise.

Thanks for reviewer's suggestions. The mean and standard deviation of the RH inside the DryNeph was $12.2 \pm 3.4\%$, we have added it in the revised marked-up manuscript at Line 145, and also shown the RH inside DryNeph in this figure (see Fig.1 [also shown in Fig. 2 in the revised marked-up manuscript]).

RH at 40% is regarded as dry. The inconsistencies at Line 140 and 219 in the revised marked-up manuscript were corrected. The potential effect of normalizing $f(RH)$ at 40% to 1 was also discussed in the revised marked-up manuscript at Line 189-198, which will underestimate the hygroscopic growth factor a few percent.

(2) The RH-cycle of 1 hour seems quite fast. Have other (longer) scan times been tested?

We don't agree with the reviewer's premise that a cycle time of 1-hours is fast, and don't understand what kind of test he/she is suggesting be performed. Numerous studies have used similar, or even faster, cycle times (Carrico et al., 1998; Koloutsou-Vakakis et al., 2001; Sheridan et al., 2001; Fierz-Schmidhauser et al., 2010a). For example, the RH scanned from ~40% to ~84% within 15 min in Carrico et al. (1998). Covert's original humidograph paper (1972) used a scan

time of 4 minutes.

(3) *Where exactly was the RH measured within the humidified nephelometer? Have the authors performed a calibration of the humidified nephelometer using a known hygroscopic substance (e.g. ammonium sulphate)?*

The RH was measured by the RH/T sensor inside the WetNeph. However, the sensor usually overestimates RH by up to 15% RH at high RH (Fierz-Schmidhauser et al, 2010a). In that case, we installed an external RH/T sensor at the outlet of the WetNeph and used it to calibrate the RH/T sensor inside the WetNeph with lamp off. The general method was to assume the T_d (dew point temperature) of RH/T sensors at the outlet of the WetNeph and inside the WetNeph to be the same (and it should be the same) and the temperature measured by the both sensors was accurate, and then using the Vaisala Humidity Calculator to retrieve the real RH inside the WetNeph. With the real RH and the measured one, the RH of the sensor inside the WetNeph was calibrated.

We have not performed the calibration using a known hygroscopic substance. However, we have calibrated the RH sensors using four well-known salts. The external RH sensors were calibrated with four saturated salt solutions (LiCl, K_2CO_3 , NaCl and $(NH_4)_2SO_4$), using the Vaisala Humidity Calibrator (HMK15) and RH/T transmitter (HMT333), which was calibrated by the National Center for Meteorological Metrology, China, in November 2012. The results were shown in Fig. 2. Good linear relationships have been achieved. Besides, the consistency of all the RH sensors have been tested, the discrepancy was <3%. Therefore, we trust the RH the RH sensors measured. We have also done the closure of scattering coefficient and scattering enhancement factor $f(RH)$ to make the measurement more trustworthy. This was described in detail in the following question.

(4) *Since there were concurrent particle size distribution measurements at the site, I strongly recommend that the results are being compared to Mie calculations using the chemical composition and size distribution measurements. This will put the results on a more trustworthy basis (see Zieger et al. (2013) for more details).*

We have done closure studies, but we did not put them in this manuscript because we are preparing to draft another manuscript focusing on the $f(RH)$ modeling. We would like to show the closure of scattering coefficient and scattering enhancement factor as follows:

Closure studies

The particle light scattering coefficient at dry and humid conditions were calculated using Mie theory with a computer code based on the work by Bohren and Huffman (2004). We assumed the particles to be spherical and homogeneously and internally mixed. As an input, the measured particle number size distribution and the complex particle refractive index n are needed. The dry particle number size distribution was measured by TDMPS and APS (see Sect. 2.2 in the manuscript); the complex particle refractive index n was derived from the chemical mass concentration measurements of the AMS and the MAAP (see Sect. 2.2 in the manuscript). A time resolved refractive index was determined by a volume fraction averaging:

$$n(\lambda) = \sum_i \frac{mf_i}{\rho_i} n_i(\lambda),$$

where mf_i is the mass fraction, ρ_i is the density and $n_i(\lambda)$ is the complex refractive index of the compound i at the wavelength of λ . The density ρ_i and the refractive index n_i of each compounds were listed in Table Response1-1 (Fierz-Schmidhauser et al., 2010b). The refractive index of

particles at humid conditions was calculated by a volume weighting of the dry refractive index n_{dry} with the refractive index of water n_{H_2O} (see Table Response1-1):

$$n_{wet} = \frac{n_{dry} + n_{H_2O}(g(RH))^3 - 1}{g(RH)^3},$$

where $g(RH)$ was the hygroscopic growth factor, defined as $g(RH)=D_{wet}(RH)/D_{dry}$, D_{dry} is the dry particle diameter and $D_{wet}(RH)$ is the diameter at a specific RH. The hygroscopic growth factor was determined by the chemical composition measurements measured by AMS and MAAP. The value of g for retrieved salts was taken from Topping et al. (2005), while BC and organics were assumed to be insoluble ($g=1$). The hygroscopic growth factor g of coarse mode particles (aerodynamic diameter $>1\mu m$) was also assumed to be 1 during the $f(RH)$ calculation (Zieger et al., 2014). The mean g was calculated with the Zdanovskii-Stokes-Robinson (ZSR) mixing rule. The one-parameter equation (Petters and Kreidenweis, 2007) was used to determine the RH dependence of $g(RH)$:

$$g(a_w) = \left(1 + \kappa \frac{a_w}{1 - a_w}\right)^{\frac{1}{3}},$$

where κ was a simple measure of the particle's hygroscopicity and a_w was the water activity, which was replaced by RH in our study, since the Kelvin effect is small for larger particles, which are relevant to the light scattering at the used wavelengths. For more details on calculation and uncertainty, please refer to Fierz-Schmidhauser et al. (2010b) and Zieger et al. (2013; 2014).

A good agreement of scattering coefficients measured by the DryNeph and calculated with Mie model at 550nm wavelength (dust-influenced episode excluded) was shown in Fig. 3. The standard deviation of 1-hour average was taken for the y-axis error, for y-axis, the uncertainty of the measurements due to the uncertainty of nephelometer was taken (Anderson et al., 1996). Figure 4 shows the predicted and calculated $f(RH, 550nm)$ at various RHs. The regression and R^2 shows good agreement of the instruments (humidification system, AMS, MAAP and TDMPS) in this study.

(5) *Page 2861, Line 10 and Figure 1: Figure 1 does not contain a real information content and could be removed. The agreement between the two nephelometers can be described within the text (e.g. by stating the result of the linear regression). Has the small difference between the two nephelometers been accounted for when calculating $f(RH)$?*

We think the reviewer was referring to Fig. 2 instead of Fig. 1. Following the reviewer's suggestion, we have removed this figure in the revised marked-up manuscript and described in Sect. 2.4 at Line 232 instead.

Yes, the small difference between the two nephelometers have been considered when calculating $f(RH)$.

2. *Page 2855, Line 28: Can the authors shortly elaborate further on how the properties of the gas and particulate matter have "changed dramatically" since 1999 at the site?*

As far as we know, there are some changes of the properties of the gas and aerosols since 1999. Firstly, according to the measurements of LinAn Regional Atmosphere background station, there is a decreasing tendency (decreased by ~15%) of PM_{10} from 2006 to 2012 in LinAn. Secondly, from 1999 to 2013, the sulfate mass concentration decreased from 21.2 ± 1.5 to 8.1 ± 4.1 (mean \pm standard deviation), partly because the Chinese government has put a high emphasize on SO_2

control. Thirdly, the SO₂ mass concentration decreased significantly from 50 to 19 μg m⁻³ at LinAn from 1999 to 2012 (ZEPB, 1999; 2012). Fourthly, the pH of rainwater of ZheJiang Province decreased from ~4.8 in 1999 to 4.17 in 2009, then increased slightly to ~4.5 in 2012 (ZEPB, 2009; 2012).

We have added some words in Line 76-77 in the revised marked-up manuscript.

3. Page 2856, Line 20: *Particles could also experience reconstruction at elevated RH (see e.g. Tritscher et al, 2011) and thus f(RH) could in theory also be slightly below 1. I suggest to rephrase, e.g. by stating "usually above 1".*

Thanks for reviewer's suggestion. Yes, we have rewritten this sentence as "f(RH,λ) and f_b(RH,λ) are always greater than 1 after water uptake (Weingartner et al., 1995)." at Line 96 in the revised marked-up manuscript.

4. *The wavelength of the MAAP is slightly different (637nm instead of 670 nm) than the manufacturer states (see Müller et al., 2011).*

Thanks, we have changed it to "637nm" and cited the paper of Müller et al (2011) at Line 176 in the revised manuscript.

5. Page 2862, Line 20: *One should not interpolate linearly to calculate f(RH)-values at different RH. The parameterizations discussed in Sect. 3.6.1 and 3.6.2. should be used instead. Generally, I think it would improve the reading if Sect. 3.6.1 and 3.6.2. are moved to the front, where the observations of f(RH) are discussed first.*

We may not express it clearly. Based on the measured RH-f(RH) curve (humidogram), we used the Matlab command "interp1(RH, f(RH), RH₀, 'linear')" to obtain f(RH₀) at the specific relative humidity RH₀, where RH and f(RH) were the RH data array and the corresponding f(RH) values, respectively, "linear" was the interpolation method we used. In fact, there are several ways of achieving f(RH₀), and we found linear interpolation was the best and easiest way to get f(RH₀) at a specific RH₀ (e.g. 80%) for our data. Firstly, parameterization were usually used to recalculate f(RH₀) (Fierz-Schmidhauser et al, 2010b; Zieger et al., 2014), however, the fitting curve of f(RH) cannot be perfectly fitted (i.e., R² won't be 1). Secondly, another way of getting f(RH₀) was to calculate the mean value of f(RH) values at RH between RH₀-ΔRH and RH₀+ΔRH (Fierz-Schmidhauser et al, 2010a; Fierz-Schmidhauser et al, 2010c; Zieger et al., 2010). This will also bring some error especially at high RH since f(RH) increases quite fast at high RH. Thirdly, as to our Humidograph schedule, the RH increased 1-3% RH every minute and we can get 28 data points from the lowest RH (~40%) to the highest RH (~90%). This data density allows us to interpolate and get more accurate f(RH₀). Fourthly, among all the ways of interpolation ('nearest', 'spline', 'cubic' and so on), linear interpolation was tested to be the best. So we choose interpolation as the method of obtaining f(RH₀).

We prefer not to move Sect. 3.6.1 and Sect. 3.6.2 to the front due to the following reasons. First, the two sections were about the parameterization and we gave the fitting parameters separately for locally-polluted, northerly-polluted and dust-influenced episodes, so this section should behind Sect. 3.4 "Classification of various observation episodes". Second, the Sect. 3.6.2 was in close relation with the following discussion of Sect. 3.6.3 Steepness of humidograms, which was a further discussion of the relationship of f(RH) and chemical compositions (Sect. 3.5), so we prefer

it behind Sect. 3.5 “The relationship of scattering enhancement factor with chemical compositions”. Considering all these factors, we prefer to leave these two sections as where they were (Sect. 3.6) and separate the discussion of the steepness index η as a new section Sect. 3.6.3 (following the reviewer’s suggestion).

6. *Figure 3: Why is RH=91% highlighted by a black line? Is this the maximum or set RH? In addition, add the RH inside the DryNeph to panel (a). Please add the wavelength to the graph or the caption.*

The black line was intended to show clearly the maximum RH (~91%). According to the reviewer’s suggestions, we have removed the black line and added the RH inside the DryNeph to panel (a) of Fig. 2 in the revised marked-up manuscript. We have also added the wavelength in the figure caption.

7. *Page 2865, Line 26: What is special about the “3 h”? This information could probably be removed.*

According to the reviewer’s suggestion, we have removed “3 h”.

8. *Page 2867, Line 16: It is not clear to the reviewer what the difference between the two affected areas are (2.8 vs. 0.27 million square kilometers). Please clarify.*

It was a strong dust event. The 2.8 million square kilometers were the total areas affected by the dust event, while the 0.27 million square kilometers only were the areas suffered from dust storms or strong sandstorms. We have rewritten this sentence as “During a severe cold air outbreak, a strong dust event struck northern China on 8 and 9 March, 2013. The affected area covered about 2.8 million square kilometers, about 0.27 million square kilometers of which suffered from dust storms or strong sandstorms” at Line 412 in the revised marked-up manuscript.

9. *Figure 4 and 8: The Ångström exponent has no unit (please remove “Å” from the figures).*

According to the reviewer’s suggestion, we removed “Å” (see Fig. 5 and 6 [also shown in Fig. 3 and 7 in the revised marked-up manuscript]).

10. *Table 5: Factor g from Zieger et al. (2014) is 0.59 ± 0.08 at 550nm (see Tab. 1 in their publication).*

We can not found g in “Influence of water uptake on the aerosol particle light scattering coefficients of the Central European aerosol” (Zieger et al., 2014), Tab. 1 in this paper was f(RH) values for 3 wavelengths.

11. *Figure 6: The panels (b) and (c) are repetitive and seen in the first panel. I suggest to just show panel (a).*

We have deleted panels (b) and (c) (see Fig. 7 [also shown in Fig. 5 in the revised marked-up manuscript]).

12. *Figure 7: Please mark which pie chart belongs to which trajectory.*

We have added ‘(a)(b)(c)’ to each pie chart, and added them in the caption (see Fig. 8 [also shown in Fig. 6 in the revised marked-up manuscript]).

13. *Figure 9: Please check the fit method, since the slope of inorganic and organic (inorganic mass fraction = 1- organic mass fraction) are not similar (the slope of the organic mass fraction should be -1 times the slope of the inorganic mass fraction). Has an orthogonal or weighted fit been used?*

The total mass concentration was calculated as the sum of mass concentrations of sulfate, nitrate, ammonium, chloride and organic measured by AMS and EBC measured by MAAP. The organic and inorganic mass fractions were calculated by dividing the mass concentration of organics (measured by AMS) and inorganic ions (the sum of sulfate, nitrate, ammonium and chloride measured by AMS) by the total mass concentration, respectively. Therefore, the sum of the organic fraction and inorganic fraction is not 1, thus the absolute value of the two slopes were not equal.

We have used the orthogonal linear fit instead of linear least square fit and drawn a new figure (see Fig. 9 [also shown in Fig. 8 in the revised marked-up manuscript]). The error of the measurements was discussed at Line 460-465 in the revised marked-up manuscript.

14. *The discussion of the steepness of the humidograms should be a separate section (following 3.6.3.). It is not really clear, if real deliquescence behaviour (so real and obvious jumps at a sudden transition from solid particle to liquid droplet) has been observed or if just the steepness increased with increasing inorganic mass fraction. Please clarify. As shown in Fig. 12b, the normalization or calculation of $f(RH)$ using the scattering coefficient at $RH=40\%$ could increase a bias in the results, since the particles could still change their water content below 40%. As mentioned above, an optical closure study using Mie theory will help to give more confidence in the measurement results.*

No deliquescence behavior was clearly observed in our study although ammonium sulfate concentration was high at sometimes. The steepness index η proposed in this study aims to provide a way of quantitatively describing the steepness of humidograms well fitted into equation $f(RH)=1+a RH^b$. The steepness decreases with the increasing of nitrate to be precise. We have separated the discussion of steepness as a new Sect. 3.6.3.

15. *The sensitivity on the direct aerosol radiative forcing is a useful exercise. However, the chosen RH of 67% as the campaign average is a bit arbitrary since the effect will be much larger at increased RH. The authors could add a figure showing the difference in radiative forcing for the entire RH range for the four cases (see e.g. Figure 8 in Fierz-Schmidhauser et al, 2010).*

The chosen RH of 67% is the mean ambient RH during the entire campaign. We used it to see the sensitivity of the direct radiative forcing of different aerosols to $f(RH)$. Following the reviewer's suggestions, we have added a figure (see Fig. 10 [also shown in Fig. 14 in the revised marked-up manuscript]) showing the influence of RH on direct forcing for the northerly-polluted period, locally-polluted period, dust-polluted period and entire campaign.

16. *The conclusions should be rewritten to really focus on the main findings. Currently, it is a repetition of sentences from the main discussion. Comparison to*

other findings with a literature discussion (e.g. sentence on Page 2875, Line 14-15) should be moved to the discussion of the results.

According to the reviewer's suggestion, we have rewritten our conclusion focusing on the main findings (see Line 630-682 in the revised manuscript). The new conclusion was follows:

“The influence of aerosol water uptake on particles' light scattering properties and direct radiative forcing have been investigated at LinAn, a regional atmospheric background station of Yangtze River Delta, China, using the scattering enhancement factor measurement system, together with AMS, MAAP and TDMPs providing the chemical composition and size distribution information. The average enhancement factors and mean standard deviations at 85% RH for scattering coefficient, backscattering coefficient and hemispheric backscatter fraction ($f(85\%)$, $f_b(85\%)$ and $f_\beta(85\%)$) were 1.58(0.12), 1.25(0.07) and 0.79(0.04), respectively. Slight wavelength dependence of $f(85\%)$ was observed at higher $f(RH)$ values. Generally, the highest values of $f(RH)$ corresponded to aged aerosols with a small fraction of OM; while the lowest values corresponded to younger aerosols with a larger fraction of OM. $f(RH)$ of aerosols with relatively low scattering coefficient was usually low with a large variation; while $f(RH)$ of aerosols with high scattering coefficients was relatively high with a small variation. Besides, NO_3^- plays an important role in determining the magnitude of $f(RH)$ at LinAn.

Humidograms measured at LinAn can be well described by the model $f(RH)=c(1-RH)^d$ and model $f(RH)=1+a \cdot RH^b$. Further investigation shows the shape of the humidogram is closely related to the mass percentage of nitrate. A steepness index η has been defined to quantitatively determine the steepness of humidograms. The more nitrate (or less sulfate), the smaller η is and the straighter the curve will be.

In March, the average relative humidity (RH_{amb}) was 67%. Consequently, the direct radiative forcing of locally-polluted, northerly-polluted and dust-influenced aerosols increased by 11.8, 19.5 and 10.5%, respectively due to aerosol uptake water in March at LinAn. At 85% RH, the direct radiative forcing increased by as high as 47% due to the aerosol hygroscopicity. In conclusion, water plays an important role in aerosol scattering properties as well as the radiative forcing, and it should be paid high attention when comparing between remote sensing and in-situ measurements and calculating the climate forcing.”

3 Technical corrections

I strongly recommend a second proof-reading regarding the English grammar. The reviewer is unable to correct all the typos, missing articles and grammar mistakes.

(1) Page 2858, Line 4: Define "SD" at its first appearance.

SD is the abbreviation for standard deviation, we have defined "SD" at its first appearance at Line 26 in the revised marked-up manuscript.

(2) Page 2857, Line 27: Replace "activated" by "active".

We think it should be "activated" charcoal, please see WIKIPEDIA via http://en.wikipedia.org/wiki/Activated_carbon.

(3) Please be consistent on how to capitalize instrument names (sometimes it is Nephelometer, sometimes nephelometer).

We have changed all the “Nephelometer” to “nephelometer”.

(4) *As a symbol for the Ångström exponent, one usually uses α as a symbol. I suggest to replace by α .*

Both symbols are used in the literature, but we prefer using “ α ” rather than “ α ” for Ångström exponent, because “ α ” is used to denote a mass scattering efficiency in this manuscript.

(5) *Page 2859, Line 26: Add the Ångström-exponent symbol at the end of the sentence.*

We have added the symbol α at the end of the sentence at Line 186 in the revised marked-up manuscript.

(6) *Page 2859, Line 23: The definition of the hemispheric backscatter fraction is a repetition and can be removed.*

We have deleted this sentence.

(7) *Page 2863, Line 12: Verb missing.*

We have changed it, Line 301 in the revised marked-up manuscript.

(8) *Page 2867, Line 13: Suggest to replace “to produce hygroscopic compounds.” by “leading to an increase in the particle’s hygroscopicity.”*

Following the reviewer’s suggestions, we have changed the sentence accordingly at Line 410 in the revised marked-up manuscript.

(9) *Page 2868, Line 6 and 7: Please add a “the” before “dust” and “Ångström”.*

We have added “the” at Line 434 and 435 in the revised marked-up manuscript.

(10) *Please add the wavelength to the captions in Tab. 1, 4, 5, 6, and 7 and as well to all figures where optical parameters are shown.*

We have added the wavelength to related Figures and Tables (Fig. 2, 3, 7, 8, 11, 14 and Table 1, 4, 5, 6 in the revised marked-up manuscript).

(11) *Figure 1: Replace “pentagram” by “star”.*

We have changed it to “star”.

References

Fierz-Schmidhauser R., Zieger P., Gysel M., Kammermann L., DeCarlo P., Baltensperger U., and Weingartner E., *Measured and predicted aerosol light scattering enhancement factors at the high alpine site Jungfraujoch*, *Atmos. Chem. Phys.*, 10(5), 2319–2333, doi:10.5194/acp-10-2319-2010, 2010.

Müller T., Laborde M., Kassell G., and Wiedensohler A., *Design and performance of a three wavelength LED-based total scatter and backscatter integrating nephelometer*, *Atmos. Meas. Tech.*, 4(6), 1291–1303, doi:10.5194/amt-4-1291-2011, 2011.

Tritscher T., Jurányi Z., Martin M., Chirico R., Gysel M., Heringa M.F., DeCarlo P.F., Sierau B., Prévôt A.S., Weingartner E., et al., *Changes of hygroscopicity and morphology during ageing of*

diesel soot, *Environmental Research Letters*, 6(3), 034026, 2011.

Zieger P., Fierz-Schmidhauser R., Weingartner E., and Baltensperger U., *Effects of relative humidity on aerosol light scattering: results from different European sites*, *Atmos. Chem. Phys.*, 13(21), 10609–10631, doi:10.5194/acp-13-10609-2013, 2013.

References in the author's response:

Bohren, C., and Huffman, D.: *Absorption and scattering of light by small particles*, Wiley-VCH, New York, USA, 2004.

Carrico, C. M., Rood, M. J., and Ogren, J. A.: *Aerosol light scattering properties at Cape Grim, Tasmania, during the first Aerosol Characterization Experiment (ACE 1)*, *J. Geophys. Res.*, 103, 16565–16574, 1998.

Covert, D. S., Charlson, R., and Ahlquist, N.: *A study of the relationship of chemical composition and humidity to light scattering by aerosols*, *J. Appl. Meteorol.*, 11, 968–976, 1972.

Fierz-Schmidhauser, R., Zieger, P., Wehrle, G., Jefferson, A., Ogren, J., Baltensperger, U., and Weingartner, E.: *Measurement of relative humidity dependent light scattering of aerosols*, *Atmos. Meas. Tech.*, 3, 39-50, 2010a.

Fierz-Schmidhauser, R., Zieger, P., Gysel, M., Kammermann, L., DeCarlo, P., Baltensperger, U., and Weingartner, E.: *Measured and predicted aerosol light scattering enhancement factors at the high alpine site Jungfraujoch*, *Atmos. Chem. Phys.*, 10, 2319-2333, 2010b.

Fierz-Schmidhauser, R., Zieger, P., Vaishya, A., Monahan, C., Bialek, J., O'Dowd, C. D., Jennings, S. G., Baltensperger, U., and Weingartner, E.: *Light scattering enhancement factors in the marine boundary layer (Mace Head, Ireland)*, *J. Geophys. Res.*, 115, D20204, doi:10.1029/2009JD013755, 2010c.

Koloutsou-Vakakis, S., Carrico, C., Kus, P., Rood, M., Li, Z., Shrestha, R., Ogren, J., Chow, J., and Watson, J.: *Aerosol properties at a midlatitude Northern Hemisphere continental site*, *J. Geophys. Res.*, 106, 3019–3032, 2001.

Petters, M., and Kreidenweis, S.: *A single parameter representation of hygroscopic growth and cloud condensation nucleus activity*, *Atmospheric Chemistry and Physics*, 7, 1961-1971, 2007.

Sheridan, P., Delene, D., and Ogren, J.: *Four years of continuous surface aerosol measurements from the Department of Energy's Atmospheric Radiation measurement Program Southern Great Plains Cloud and Radiation Testbed site*, *J. Geophys. Res.*, 106, 20735-20747, 2001.

Weingartner, E., Baltensperger, U., and Burtscher, H.: *Growth and structural change of combustion aerosols at high relative humidity*, *Environ. Sci. Tech.*, 29, 2982-2986, 1995.

Zhejiang Environmental Protection Bureau (ZEPB), 2006, *Annual Report on the State of the Environment of Zhejiang Province*, Zhejiang Environmental Protection Bureau, Hangzhou, 17 pp., 1999.

Zhejiang Environmental Protection Bureau (ZEPB), 2006, *Annual Report on the State of the Environment of Zhejiang Province*, Zhejiang Environmental Protection Bureau, Hangzhou, 29 pp., 2009.

Zhejiang Environmental Protection Bureau (ZEPB), 2006, *Annual Report on the State of the Environment of Zhejiang Province*, Zhejiang Environmental Protection Bureau, Hangzhou, 29 pp., 2012.

Zieger, P., Fierz-Schmidhauser, R., Gysel, M., Ström, J., Henne, S., Yttri, K. E., Baltensperger, U.,

and Weingartner, E.: Effects of relative humidity on aerosol light scattering in the Arctic, *Atmos. Chem. Phys.*, 10, 3875-3890, 2010.

Zieger P., Fierz-Schmidhauser R., Weingartner E., and Baltensperger U., Effects of relative humidity on aerosol light scattering: results from different European sites, *Atmos. Chem. Phys.*, 13(21), 10609–10631, doi:10.5194/acp-13-10609-2013, 2013.

Zieger, P., Fierz-Schmidhauser, R., Poulain, L., Müller, T., Birmili, W., Spindler, G., Wiedensohler, A., Baltensperger, U., and Weingartner, E.: Influence of water uptake on the aerosol particle light scattering coefficients of the Central European aerosol, *Tellus B*, 66, 22716, doi: 10.3402/tellusb.v66.22716, 2014.

Table Response1-1 Microphysical properties of selected aerosol compounds used for the model predictions. The imaginary part of the complex refractive index n was omitted for all components except for black carbon (BC). All values are in 550nm wavelength.

| | $(\text{NH}_4)_2\text{SO}_4$ | NH_4NO_3 | OM | BC | H_2O |
|--------|------------------------------|--------------------------|------|------------|----------------------|
| n | 1.530 | 1.556 | 1.48 | 1.75+0.44i | 1.333 |
| ρ | 1.77 | 1.72 | 1.4 | 1.7 | 1 |

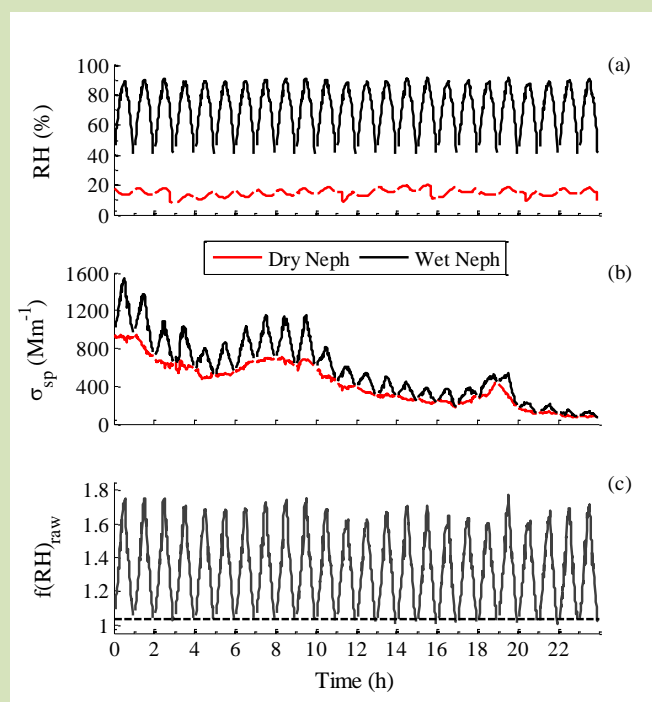


Fig. 1 Example of recorded data on 17 March 2013 (a) Relative humidity inside DryNeph (red line) and WetNeph (black line); (b) Aerosol scattering coefficients measured by DryNeph (red line) and WetNeph (black line) at 550nm wavelength; (c) Raw scattering enhancement factor $f(\text{RH}, 550\text{nm})_{\text{raw}}$ without normalization, the black dash line was $f(\text{RH})_{\text{raw}}=1.03$.

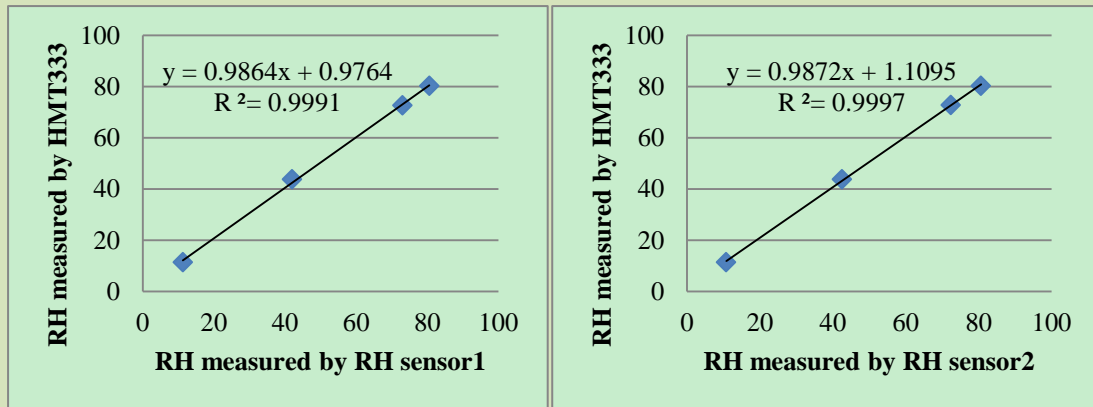


Fig. 2 The calibration of RH sensors. Sensor 1 was the external RH/T sensor (wetout) at the outlet of the WetNeph and sensor 2 was another external RH/T sensor at the inlet of the DryNeph. Sensor 1 and 2 were measured at 22.7 and 22.3 °C, respectively.

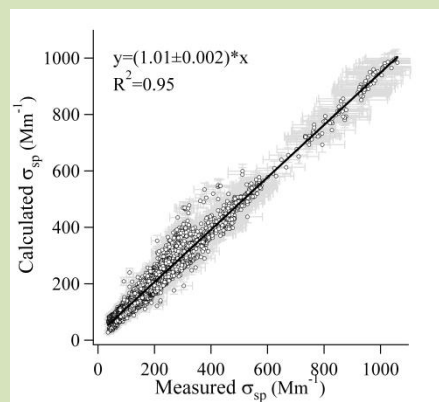


Fig. 3 Comparison of measured scattering coefficients and calculated scattering coefficients at 550nm wavelength (dust-influenced episode excluded). The error bars gave the standard deviation of the calculated σ_{sp} and the uncertainty of the measured σ_{sp} .

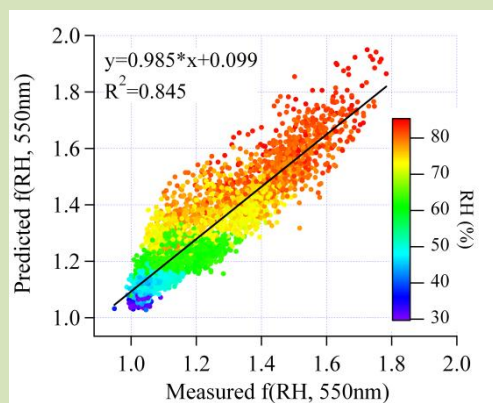


Fig. 4 Predicted and modeled $f(RH, 550nm)$ for various RHs. The black solid line represents the linear least square regression.

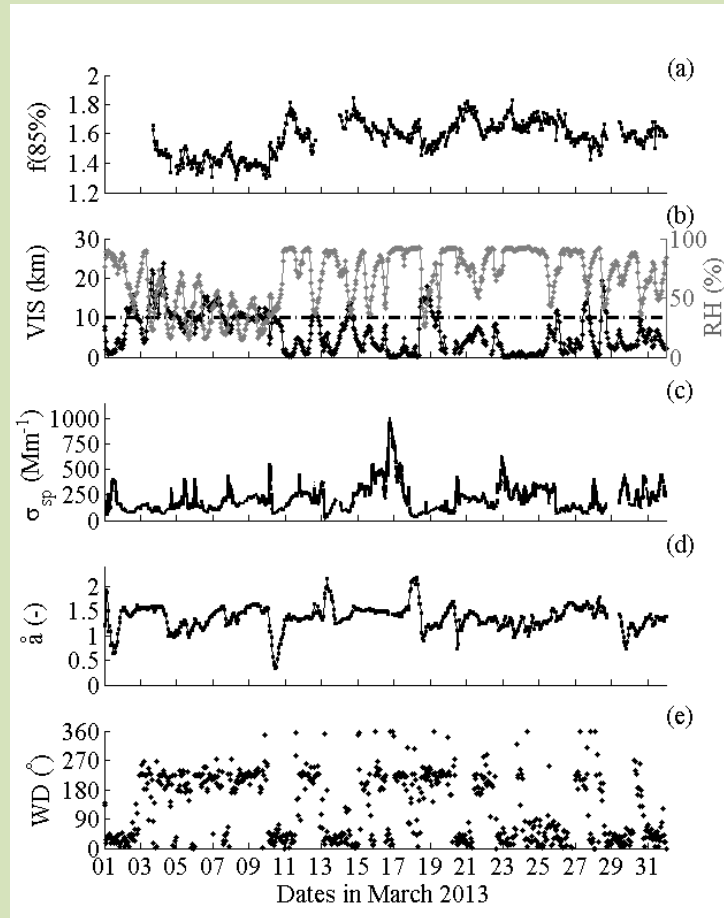


Fig. 5 Time series of measured and derived aerosol variables, as well as the ambient RH and visibility. (a) scattering enhancement factor $f(85\%)$ at 550 nm wavelength; (b) visibility (VIS) and relative humidity (RH) at ambient conditions, the dashed line represents $VIS=10$ km; (c) aerosol scattering coefficient of DryNeph at 550 nm wavelength; (d) Ångström exponent \hat{a} (e) wind direction (WD), indicating prevailing wind directions during observation period was mainly northeasterly (NE) and southwesterly (SW).

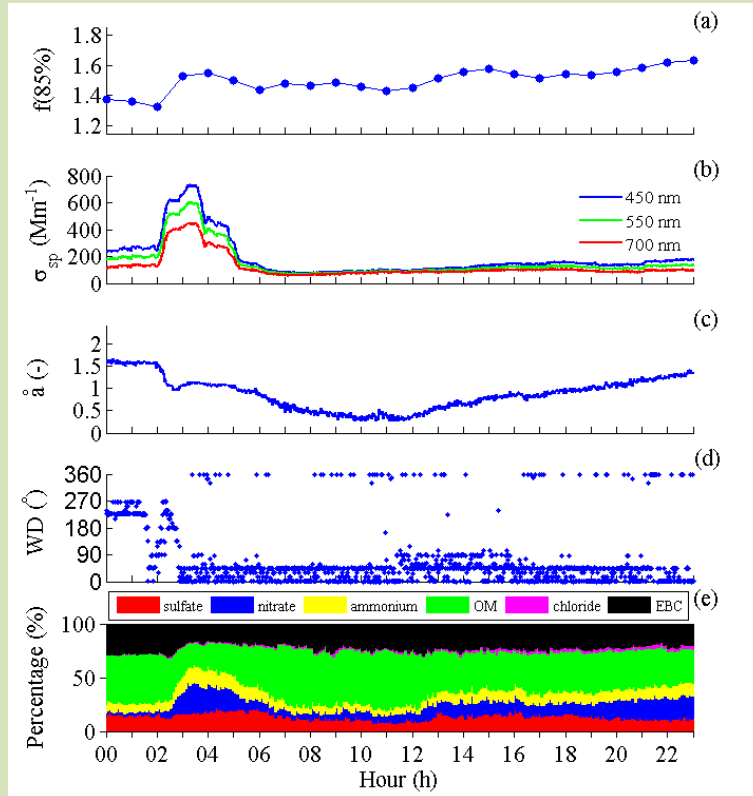


Fig. 6 Parameters in episode influenced by dust on 10 March 2013 at LinAn (a) scattering enhancement factor $f(85\%)$ at 550nm; (b) scattering coefficients at 450nm, 550nm and 700nm wavelengths; (c) Ångström exponent \tilde{a} (d) wind direction; (e) mass percentages of chemical species measured by AMS and MAAP.

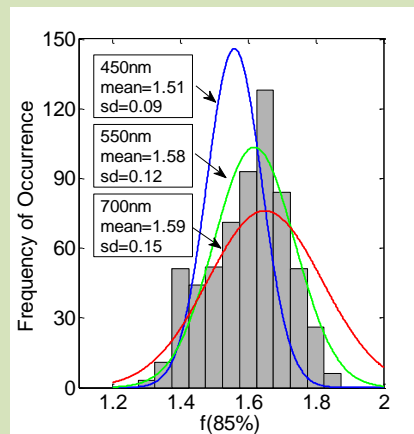


Fig. 7 Histogram of $f(85\%,550 \text{ nm})$ overlaid with the Gaussian curves based on the statistics for $f(85\%,450 \text{ nm})$, $f(85\%,550 \text{ nm})$ and $f(85\%,700 \text{ nm})$.

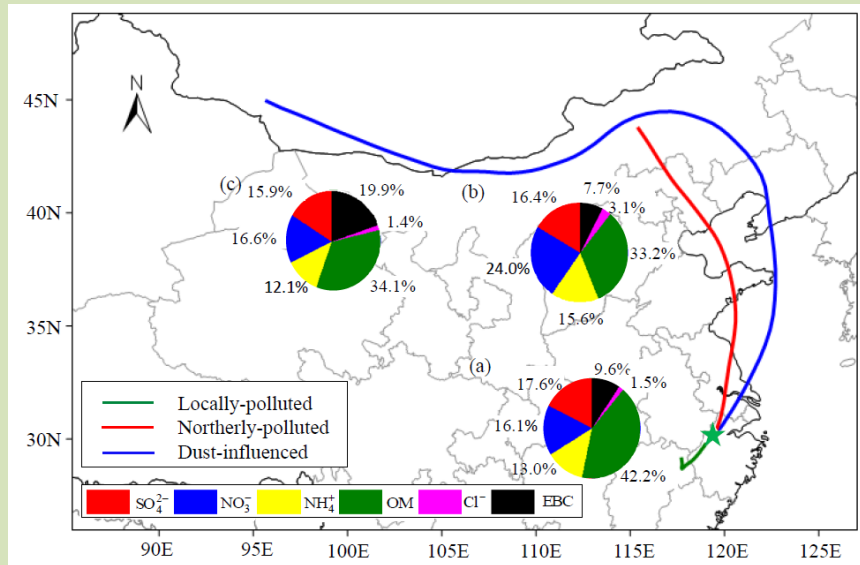


Fig. 8 72h back trajectories of locally-polluted period, northerly-polluted period and dust-influenced period, together with the mean mass fraction of submicron chemical compositions (SO₄²⁻, NO₃⁻, NH₄⁺, OM and Cl⁻) measured by AMS and EBC in PM₁₀ measured by MAAP. The pie chart (a), (b) and (c) were for locally-polluted, northerly-polluted and dust-influenced periods, respectively.

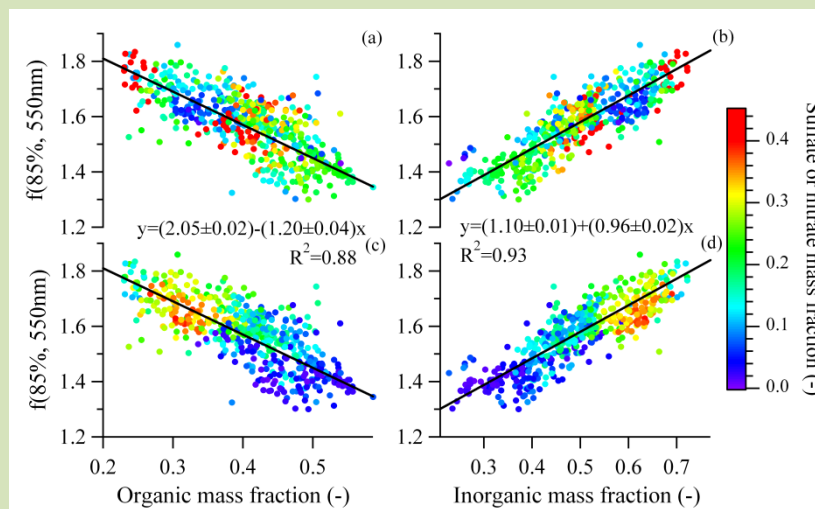


Fig. 9 Scattering enhancement factor $f(85\%, 550\text{nm})$ vs. organic mass fraction and inorganic mass fraction determined from AMS and MAAP: (a) (b) $f(85\%, 550\text{nm})$ vs. organic mass and inorganic mass fraction colored by sulfate mass fraction, respectively; (c) (d) $f(85\%, 550\text{nm})$ vs. organic mass fraction and inorganic mass fraction colored by nitrate mass fraction, respectively. The solid black line represent a bivariate linear regression including the uncertainty of $f(85\%, 550\text{nm})$ and the standard deviation of chemical compositions.

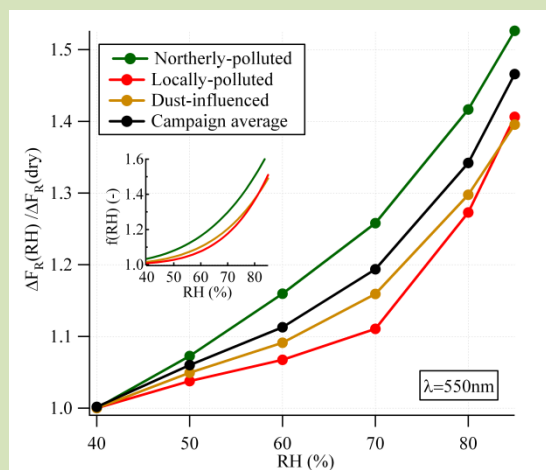


Fig. 10 Influence of relative humidity (RH) on direct radiative forcing for the entire campaign (black line), as well as for the northerly-polluted, locally-polluted and dust-polluted periods, measured by the ratio of radiative forcing at a certain RH to that at dry conditions. The small inlay shows the fitting curves of $f(\text{RH})$ for northerly-polluted, locally-polluted and dust-polluted periods, respectively, using fitting parameters in Table 6. All the parameters were measured at 550nm.

Comments from Referee #2

The contribution contains original measurements, taken in China.

I suggest minor revisions.

Thanks for reviewer's suggestions. We have revised the manuscript accordingly.

1. *Abstract should contain the goal of the paper, the techniques used, and the main results.*

The techniques applied are missing.

Following the reviewer's suggestion, we have added the techniques applied in our study and rewritten the second sentence in the abstract as:

"To achieve a better understanding of the effect of aerosol hygroscopic growth on light scattering properties and radiative forcing, the aerosol scattering coefficients at RH varying from 40% to ~90% was measured using the humidification system (consists of a nephelometer and a humidified nephelometer) in the Yangtze River Delta of China in March 2013. In addition, the aerosol size distribution and chemical composition were measured."(see Line 21-25 in the revised marked-up manuscript).

2. *Page 2856, line 20: larger than one, (greater is frequently used in the paper, but larger is appropriate).*

We asked help from native English co-author. The suggestions are: "Greater" and "larger" are two words we should pay attention to. Usually, "greater" is used when referring to values, and "larger" (or "bigger", of course) when referring to the size of entities (whether physical or abstract). So, we revised the manuscript accordingly. For example, there are places we have

misused “greater” (Line 26 of p.2871; Line 9 and 17 p.2872), we have changed them to “larger” in the revised marked-up manuscript (Line 544 and 555).

3. *Page 2858, line 9: So, you humidify the aerosol from very dry conditions to RH 40% (for neph #1) and then to the elevated RH (for neph #2)? Please clarify!*

The aerosols pass through an aerosol dryer, enter the DryNeph, and then WetNeph. The measured RH inside DryNeph was always below 20% RH (see Fig.1 [also shown in Fig. 2 in the revised marked-up manuscript]). There is a humidifier between DryNeph (neph #1) and WetNeph (neph #2), which controls the RH of aerosols entering the WetNeph (neph #2). The humidifier set point is stepped from ~40% to ~90% RH during the first half hour, and back to ~40% RH during the last half hour (see Fig.1 [also shown in Fig. 2 in the revised marked-up manuscript]). For example, at 03min, the RH set point was 40%, the aerosols were humidified directly from <20% to 40% RH; at 30min, the RH set point was 90%, aerosols were humidified directly from <20% to ~90% RH. Each minute correspond to a different RH set point, so that a RH cycle was obtained.

4. *Page 2862, line 9: 20 to 1000 Mm-1 corresponds to 4-200 km visibility, and not to 0.1 to 23.7 km as in Fig 4b. Please clarify!*

Yes, you are right if it was the ambient scattering coefficient. However, the scattering coefficients were measured under dry conditions, while the visibility was measured under ambient conditions. There was an automatic regenerating adsorption aerosol dryer at the inlet to provide dry air for all the instruments. The scattering coefficients, number size distribution and the masses of chemical compositions were all measured under dry conditions. We have added “under dry conditions” at Line 263 in the revised marked-up manuscript to make it clear.

5. *Page 2863, paragraph, line 3-16: What about the impact (changes)... when the particles are dried and when they get wet again, ... Does that not also influence the determination of the enhancement factor? Could be discussed?*

Transport losses, thermophoresis, coagulation, evaporation, and irreversible chemical reactions and so on can differentiate the particles from the original ones, and thus impact the $f(\text{RH})$. However, drying and humidifying is necessary. For one thing, measuring aerosol properties at dry conditions can make the data comparable; for another, only if the particles are dried and humidified can we get the scattering enhancement factor $f(\text{RH})$ since it is defined as $f(\text{RH}) = \sigma_{\text{sp}}(\text{RH}) / \sigma_{\text{sp}}(\text{dry})$. In that case, we have made an effort to retain the aerosol property. For example, the transport path was made as short and straight as possible, particle-free air was diluted to the aerosol stream to reduce coagulation, and lower RH and higher heater temperature was avoided as it will result in semi volatile compounds like weak organic acids and nitrates evaporating from the aerosol.

6. *Table 5 According to the old work of Haenel in the 1980ies and subsequent work, c and g is in the range from 0.4-0.9 and g from about 0.6-0.9. But you find c=1.000? and g below 0.3? Can you discuss that?*

Furthermore, one can compute gamma from c and g (see Haenel, 1984), and he found

values of gamma around 0.4, but you get rather low gammas below 0.2? How can one explain that?

Table 5 in this manuscript shows the fitting parameter (c and g) of f(RH) with equation $f(RH)=c(1-RH)^{-g}$. The parameters c and g both determine the magnitude of f(RH). The larger the g and c parameters are, the larger the f(RH) will be. The parameter g determines the curvature of humidograms (f(RH)-RH curve). The larger g is, the bigger the curvature will be. Figure 2 show how the f(RH) varies with the parameter c and g. As is shown, the influence of g on the magnitude of f(RH) is more important than that of c. The parameter c and g in this study was ~0.9 and ~0.3, respectively, since the f(RH) value (e.g. f(80%) = 1.44±0.12) was comparably lower than most of the f(RH) values obtained in Europe, USA, the Arctic and so on. The value of c and g of LinAn was similar to these obtained by Gasso (2000) during a dust event with the f(RH) value f(80%) = 1.33±0.07. Hänel (1984) found the empirical models of f(RH) for background aerosols were $f(RH)=(1-RH)^{-0.4364}$ (RH<70%) and $f(RH)=0.6130*(1-RH)^{-0.6118}$ (70%<RH<99.9%), for urban aerosols were $f(RH)=(1-RH)^{-0.2053}$ (RH<70%) and $f(RH)=0.7008*(1-RH)^{-0.7317}$ (70%<RH<99.9%). The relatively larger value of parameter g at higher RH indicates the rapid increase of f(RH) with RH increase (as shown in Fig. 3), while the humidograms in our study were different, the f(RH) values were not as large as those obtained by Hänel (1984). In conclusion, the parameter c and g are dependent on the humidogram (both its curvature and the magnitude of f(RH)), the relatively low g value obtained in our study indicates the f(RH) is lower in this study, which is determined by the aerosol chemical composition, particle size distribution and so on.

7. *Figure 1, I see a green star!*

We have changed the word “pentagram” to “star”.

8. *Figure 3, a (as very thin green line) and b in one plot may help, but separately plotted, Figure 3a makes no sense, can be skipped.*

We want to show the performance of our humidification measurement system on the RH control, which is a very important part of our experiment. In order to shown more information in this figure, we have added the RH inside the DryNeph to panel (a) and added the ratio of $\sigma_{sp,wet}/\sigma_{sp,dry}$ (f(RH)_{raw} value) as panel (c) (see Fig.1 [also shown in Fig. 2 in the revised marked-up manuscript]). Hope this will make this figure more meaningful.

9. *Figure 4 contains the essential results. This figure must be large! Is the information on wind useful? Otherwise leave out. And all periods which are discussed in more detailed should be highlighted in the plot (grey shading or so).*

According to the reviewer’s suggestion, we have redrawn this figure. We have enlarged the size of the figure and used larger font size (see Fig. 4 [also shown in Fig. 3 in the revised marked-up manuscript]).

We have classified the whole month period into three episodes: the locally-polluted period, the northerly-polluted period and the dust-influenced period. The criteria of the classification were the wind direction, back trajectory and weather phenomenon. We have thought about highlighting the three periods, however, there are cases when the northerly-polluted period only last for several hours, and then changed to the locally-polluted period, if we highlight

them all, the figure would be a little messy. So we have not highlighted the three periods in the plot.

10. Figure 6: The found histogram (FoO) in (a) has no Gaussian shape, why do you then show, in addition, Gaussian curves?

Yes, the distribution of the occurrence of $f(85\%)$ was not an exact Gaussian distribution. But as Pearson once said, "I can only recognize the occurrence of the normal curve - the Laplacian curve of errors - as a very abnormal phenomenon. It is roughly approximated to in certain distributions; for this reason, and on account for its beautiful simplicity, we may, perhaps, use it as a first approximation, particularly in theoretical investigations". In our study, Gaussian curves captures the main characteristics of the distribution of the occurrence of $f(85\%, 450\text{nm})$, $f(85\%, 550\text{nm})$ and $f(85\%, 700\text{nm})$ with R^2 of 0.98, 0.94 and 0.92, respectively. Besides, we use the Gaussian fitting curve as a representation of the data so that we could put the three lines together to make the comparison more clearly.

References in the author's response:

- Gasso, S., Hegg, D., Covert, D., Collins, D., Noone, K., Öström, E., Schmid, B., Russell, P., Livingston, J., and Durkee, P.: Influence of humidity on the aerosol scattering coefficient and its effect on the upwelling radiance during ACE - 2, *Tellus B*, 52, 546-567, 2000.
- Hänel, G.: Parameterization of the influence of relative humidity on optical aerosol properties, *Aerosols and Their Climatic Effects*, 117-122, 1984.
- Zieger, P., Fierz-Schmidhauser, R., Gysel, M., Ström, J., Henne, S., Yttri, K. E., Baltensperger, U., and Weingartner, E.: Effects of relative humidity on aerosol light scattering in the Arctic, *Atmos. Chem. Phys*, 10, 3875-3890, doi:10.5194/acp-10-3875-2010, 2010.

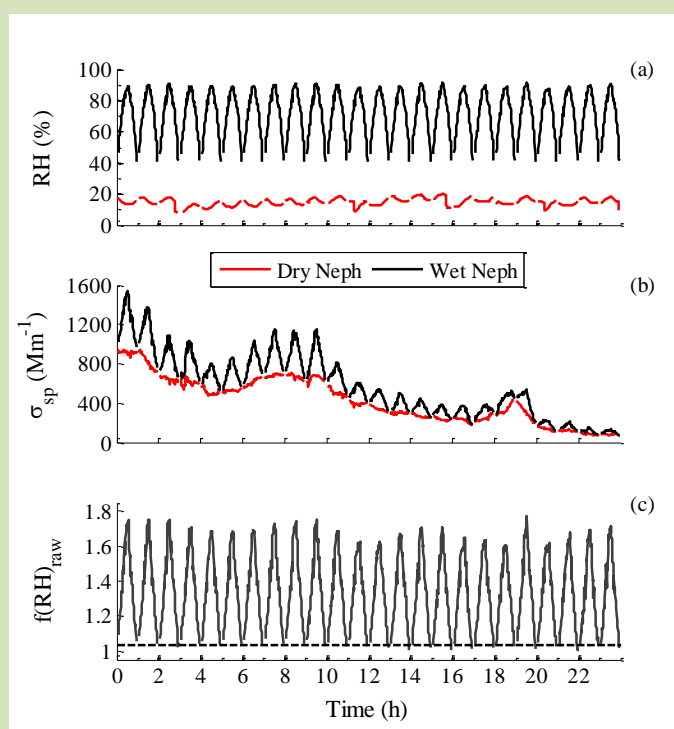


Fig. 1 Example of recorded data on 17 March 2013 (a) Relative humidity inside DryNeph (red line) and WetNeph (black line); (b) Aerosol scattering coefficients measured by DryNeph (red line) and WetNeph (black line) at 550nm wavelength; (c) Raw scattering enhancement factor $f(\text{RH}, 550\text{nm})_{\text{raw}}$ without normalization, the black dash line was $f(\text{RH})_{\text{raw}}=1.03$.

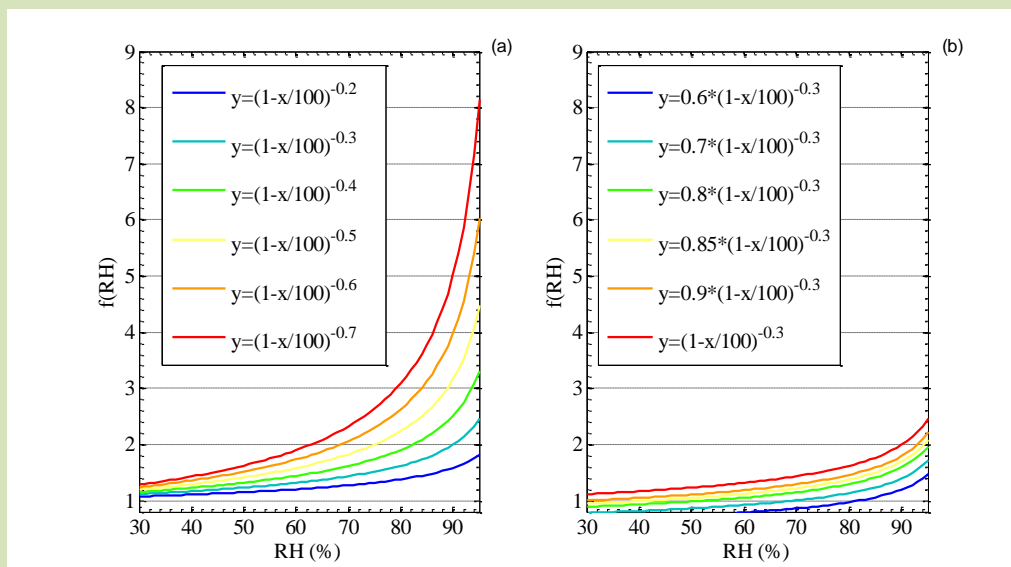


Fig. 2 Sample curves of $f(\text{RH})=c*(1-\text{RH})^{-g}$ with various c and g .

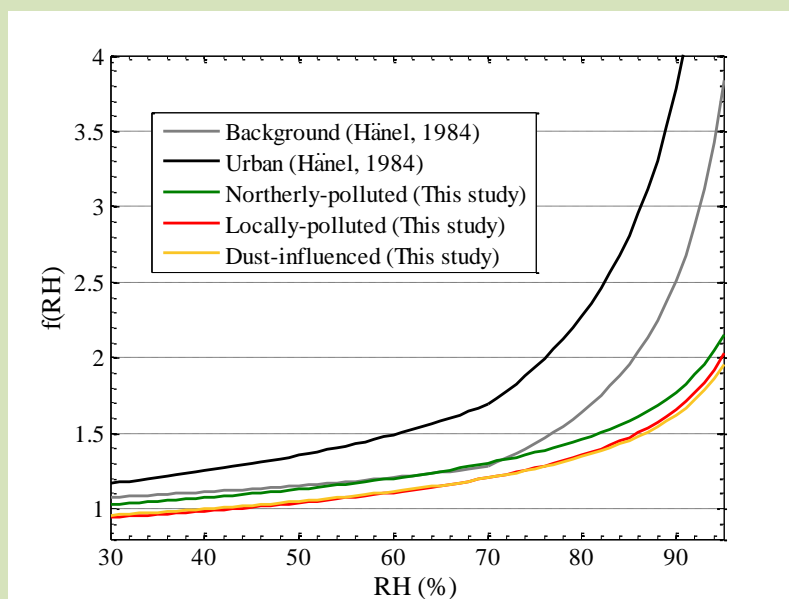


Fig. 3 Fitting curves of humidograms of Hänel and this study.

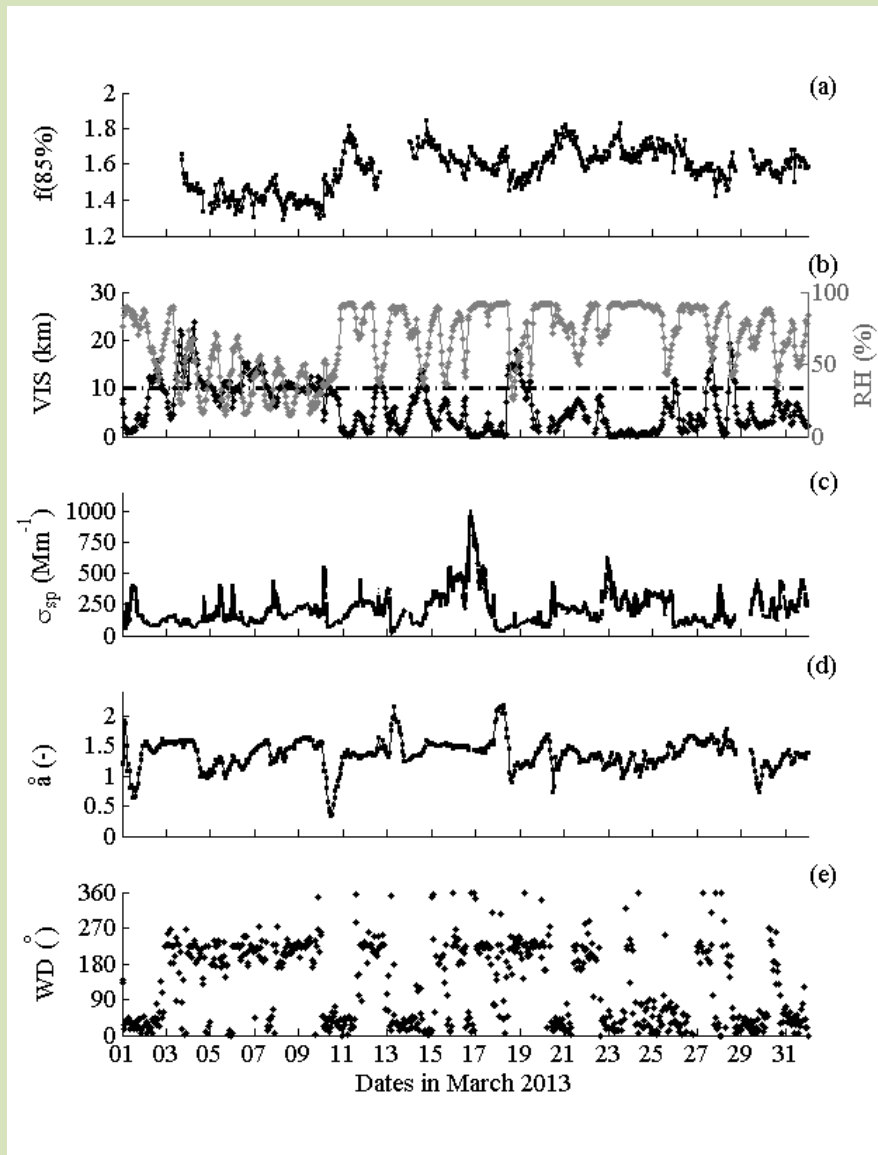


Fig. 4 Time series of measured and derived aerosol variables, as well as the ambient RH and visibility. (a) scattering enhancement factor $f(85\%)$ at 550 nm wavelength; (b) visibility (VIS) and relative humidity (RH) at ambient conditions, the dashed line represents $VIS=10$ km; (c) aerosol scattering coefficient of DryNeph at 550 nm wavelength; (d) Ångström exponent α (e) wind direction (WD), indicating prevailing wind directions during observation period was mainly northeasterly (NE) and southwesterly (SW).

The marked-up manuscript:

1

1 Observations of relative humidity effects on aerosol light 2 scattering in the Yangtze River Delta of China

3 Zhang Lu^{1,2}, Sun Junying^{1,3}, Shen Xiaojing¹, Zhang Yangmei¹, Che Haochi¹,

4 Ma Qianli⁴, Zhang Yiwen¹, Zhang Xiaoye¹, John A. Ogren⁵

5 ¹ Key Laboratory of Atmospheric Chemistry of CMA, Institute of Atmospheric
6 Composition, Chinese Academy of Meteorological Sciences, Beijing 100081, China

7 ² College of Earth Science, University of Chinese Academy of Sciences, Beijing
8 100049, China

9 ³ State Key Laboratory of Cryospheric Sciences, Cold and Arid Region
10 Environmental and Engineering Research Institute, Chinese Academy of Sciences,
11 Lanzhou 730000, China

12 ⁴ LinAn Regional Atmosphere Background Station, LinAn 311307, China

13 ⁵ Earth System Research Laboratory, NOAA, Boulder, CO, USA

14 Correspondence to: J.Y. Sun (jysun@cams.cma.gov.cn)

15
16 **Abstract**

17 Scattering of solar radiation by aerosol particles is highly dependent on relative
18 humidity (RH) as hygroscopic particles take up water with increasing RH. To achieve
19 a better understanding of the effect of aerosol hygroscopic growth on light scattering
20 properties and radiative forcing, ~~a field campaign was carried out~~ the aerosol scattering
21 coefficients at RH in the range of 40% to ~90% was measured using the
22 humidification system (consists of two nephelometers operating in series with a
23 humidifier in between) in the Yangtze River Delta of China in March 2013. In
24 addition, the aerosol size distribution and chemical composition were measured.

25 During the observation period, the mean and standard deviation (SD) of enhancement
26 factors at RH=85% for the scattering coefficient ($f(85\%)$), backscattering coefficient
27 ($f_b(85\%)$) and hemispheric backscatter fraction ($f_\beta(85\%)$) were 1.58 ± 0.12 , 1.25 ± 0.07
28 and 0.79 ± 0.04 , respectively, i.e. aerosol scattering coefficient and backscattering
29 coefficient increased by 58 and 25% as the RH increased from 40 to 85%. Meanwhile,
30 the aerosol hemispheric backscatter fraction decreased by 21%. The relative amount
31 of organic matter (OM) ~~and-or~~ inorganics in PM_1 was found to be a main factor
32 determining the magnitude of $f(RH)$, the highest values of $f(RH)$ corresponded to the

33 aerosols with a small fraction of OM, and vice versa. The relative amount of NO_3^- in
34 fine particles was strongly correlated to $f(85\%)$, which suggests NO_3^- played a vital
35 role in aerosol hygroscopic growth during this study. The mass ~~percentage~~ fraction of
36 nitrate also had a close relation to the curvature of humidograms, namely, the higher
37 the nitrate concentration is, the straighter the humidogram will be. At 85% RH, the
38 aerosol direct radiative forcing increased by 47% compared to that in dry conditions
39 due to the aerosol hygroscopic growth. Air masses that arrived at LinAn in March can
40 be classified into northerly polluted, locally polluted and dust influenced types, the
41 scattering enhancement factors at 85% RH were 1.52 ± 0.10 , 1.64 ± 0.09 and 1.48 ± 0.05 ,
42 respectively. The sensitivity of the aerosol radiative forcing to $f(\text{RH})$ at the measured
43 mean ambient RH 67 % for various aerosol types was also estimated. The direct
44 radiative forcing increased by 11.8, 19.5 and 10.5%, respectively, for locally polluted,
45 northerly polluted and dust influenced aerosols due to aerosol hygroscopic growth at
46 LinAn in March 2013.

47 **1 Introduction**

48 Hygroscopic aerosols take up water as humidity increases (Engelhart et al.,
49 2011;Pilinis et al., 1989;H änel, 1976;Covert et al., 1972). Aerosol water matters since
50 water can affect both the size and refractive indices of atmospheric aerosols, thereby
51 influencing the mass concentration, size distribution, and corresponding optical
52 properties (e.g., scattering coefficient, backscattering coefficient, single scattering
53 albedo, and asymmetry parameter) (Cheng et al., 2008;Randles et al., 2004;Malm et
54 al., 2003;Carrico et al., 2003). In particular, understanding the effect of relative
55 humidity on aerosol light scattering is important to better estimate the radiative
56 forcing and evaluate visibility impairment (Ackerman et al., 2004;Tang,
57 1996;Charlson et al., 1992;Covert et al., 1972). Besides, most of the ground-based
58 aerosol measurements are conducted in dry conditions so as to have a consistency
59 within networks. These measurements can differ significantly from the ambient ones.
60 Thus, the determination of enhancement factors for various optical variables are of
61 crucial importance for climate forcing calculations (Quinn et al., 1995;Pilinis et al.,

62 1995) and the comparison between remote sensing and ground based measurements
63 (Zhang et al., 2012;Wang and Martin, 2007;Zieger et al., 2012).

64 The Yangtze River Delta, one of the most populated and fastest growing regions
65 in China, has experienced extraordinary economic growth during the last two decades.
66 Amounting to 2.1% of the land area of China, this region contains ~11% of the
67 country's population and produces ~20% of China's Gross Domestic Product (GDP)
68 in 2013 (Wang et al., 2013). Concurrent with population increase and economic
69 growth are the increasing energy consumption and growing number of automobiles,
70 and therefore, the Yangtze River Delta has become a significant source of gas and
71 particulate pollutants and secondary aerosol production. A 5-week field campaign was
72 carried out in the early winter of 1999 at LinAn, a background station in the Yangtze
73 River Delta (Xu et al., 2002). However, since then the physical and chemical
74 properties of gas and particulate pollutants have changed dramatically with the rapidly
75 developing economy and fast growing population, e.g. from 1999 to 2013, the sulfate
76 mass concentration decreased from 21.2±11.5 to 8.1±4.1 (mean ± SD) (Qi et al.,
77 2012;Xu et al., 2008;ZEPB, 1999;ZEPB, 2013). In order to better understand the
78 aerosol light scattering properties and their dependency on relative humidity in the
79 Yangtze River Delta, both the scattering and backscattering coefficients under dry
80 (RH<~~30~~40%) conditions and controlled relative humidity were measured, along with
81 the chemical composition and particle number size distribution.

82 The enhancement factors discussed in this work include scattering enhancement
83 factor $f(\text{RH},\lambda)$, enhancement factor for backscattering coefficient $f_b(\text{RH},\lambda)$ and
84 enhancement factor for hemispheric backscatter fraction $f_\beta(\text{RH},\lambda)$. The impact of
85 relative humidity on the aerosol light scattering coefficient is defined as scattering
86 enhancement factor $f(\text{RH},\lambda)$:

$$87 \quad f(\text{RH},\lambda) = \sigma_{\text{sp}}(\text{RH},\lambda) / \sigma_{\text{sp}}(\text{dry},\lambda) \quad (1)$$

88 where $\sigma_{\text{sp}}(\text{dry},\lambda)$ and $\sigma_{\text{sp}}(\text{RH},\lambda)$ represent scattering coefficients at wavelength λ in dry
89 conditions and at a defined higher relative humidity, respectively.

90 Likewise, the impact of relative humidity on aerosol backscattering coefficient

91 can be described as enhancement factor for backscattering coefficient $f_b(\text{RH}, \lambda)$:

$$92 \quad f_b(\text{RH}, \lambda) = \sigma_{\text{bsp}}(\text{RH}, \lambda) / \sigma_{\text{bsp}}(\text{dry}, \lambda) \quad (2)$$

93 where $\sigma_{\text{bsp}}(\text{dry}, \lambda)$ and $\sigma_{\text{bsp}}(\text{RH}, \lambda)$ represent backscattering coefficients at wavelength λ
94 in dry conditions and at a defined relative humidity, respectively. $f(\text{RH}, \lambda)$ and $f_b(\text{RH}, \lambda)$
95 are always greater than 1 if no significant restructuring is taken place after water
96 uptake (Weingartner et al., 1995).

97 Hemispheric backscatter fraction (b) is closely related to the upscatter fraction
98 ($\bar{\beta}$), the fraction of incident solar radiation scattered into space (Wiscombe and Grams,
99 1976). The impact of relative humidity on aerosol hemispheric backscatter fraction
100 can be defined as enhancement factor for hemispheric backscatter fraction $f_\beta(\text{RH}, \lambda)$
101 (Adam et al., 2012):

$$102 \quad f_\beta(\text{RH}, \lambda) = b(\text{RH}, \lambda) / b(\text{dry}, \lambda) \quad (3)$$

103 where $b(\text{dry}, \lambda)$ and $b(\text{RH}, \lambda)$ represent hemispheric backscatter fraction at wavelength
104 λ in dry conditions and at the defined relative humidity. b is defined as the ratio of
105 backscattering coefficient to scattering coefficient: $b = \sigma_{\text{bsp}} / \sigma_{\text{sp}}$. Thus, $f_\beta(\text{RH}, \lambda)$ can be
106 rewritten as: $f_\beta(\text{RH}, \lambda) = f_b(\text{RH}, \lambda) / f(\text{RH}, \lambda)$.

107 The wavelength dependence of scattering enhancement factor $f(\text{RH}, \lambda)$ varies
108 with generalized aerosol types. Kotchenruther and Hobbs (1998) and Zieger et al.
109 (2010; 2011) found no pronounced wavelength dependence of $f(\text{RH}, \lambda)$ for biomass
110 burning aerosols and arctic aerosols, respectively; Zieger et al. (2013) found small
111 variations (<5%) of $f(\text{RH}, \lambda)$ at 450, 550 and 700 nm for several European sites;
112 Kotchenruther et al. (1999) and Magi and Hobbs (2003) reported significant
113 wavelength dependence of $f(\text{RH}, \lambda)$ for urban/industrial aerosols off the east coast of
114 the United States. In this study, the wavelength dependence of enhancement factors
115 was also investigated. Except when specially mentioned, all the parameters discussed
116 in this study are based on the measurements at 550 nm wavelength only.

117

118 **2 Experimental sites and instrumentation**

119 **2.1 Site description**

120 This study was carried out during an intensive field sampling period from 1 to 31
121 March 2013 at LinAn Regional Atmosphere background station, which is a WMO
122 GAW regional station (30.3° N, 119.73° E, 138 m a.s.l.) located in the center of
123 Yangtze River Delta, China (Fang et al., 2013) (as shown in Fig. 1). It is
124 approximately 11 km north of the city of LinAn, with a population of 1.5 million. The
125 site is ~50 km west of Hangzhou (capital of Zhejiang Province with a population of
126 ~8.8 million) and ~210 km southwest of Shanghai (a mega-city with a population of
127 ~20 million). LinAn station is on the top of a small hill, in an area primarily covered
128 by bamboo forests and paddy rice fields, and represents the background conditions of
129 the Yangtze River Delta. North of the station is a small village with ~200 inhabitants.
130 In addition, there is an activated charcoal factory ~1.4 km north of LinAn station that
131 uses bamboo wood as its source material (Qi et al., 2012). During the observation
132 period, the prevailing winds were northeasterly (NE) and southwesterly (SW) with an
133 average wind speed of $\sim 2.5 \text{ m s}^{-1}$ (SD 1.4 m s^{-1}). 72-hour back trajectories showed two
134 contrasting air mass origins: (1) air masses from Northern China through
135 long-distance transport and (2) air masses from southerly/southwesterly directions
136 with a much shorter transport distance.

137 2.2 Measurement system and data processing

138 The scattering enhancement factor $f(\text{RH})$ is defined as the ratio of aerosol
139 scattering coefficient at a given, elevated RH to that at a low RH (usually <34%).
140 Correspondingly, the measurement—humidification system included two
141 nephelometers operating in series with a humidifier between them. Sample air entered
142 the first nephelometer (reference nephelometer or DryNeph) through an aerosol dryer
143 (Shen et al., 2011; Tuch et al., 2009) to ensure the aerosol was at dry conditions (RH
144 inside DryNeph was $12.2 \pm 3.4\%$ (mean \pm SD) for the whole field campaign), where
145 the sample RH was controlled to <30%, then passed through the humidifier, where the
146 sample RH was regulated to a higher RH that was ramped from ~40 to 90%, and
147 finally entered the second nephelometer (humidified nephelometer or WetNeph)
148 where the scattering coefficient of humidified aerosols was measured.

149 Aerosol total scattering (between 7 and 170 degrees) and backscattering

150 coefficients (between 90 and 170 degrees) were measured by an [Integrating](#)
151 [integrating Nephelometer-nephelometer](#) (TSI Inc., Model 3563) at three wavelengths:
152 blue (450 nm), green (550 nm) and red (700 nm). Data were recorded as 1-minute
153 average and a zero check was performed automatically once per hour. The detailed
154 information of this instrument has been described in many previous studies (Anderson
155 and Ogren, 1998; Charlson et al., 1969; Anderson et al., 1996).

156 The humidifier was built by the aerosol group in Global Monitoring Division,
157 Earth System Research Laboratory, National Ocean & Atmospheric Administration,
158 USA (NOAA/GMD), which was described in Carrico et al. (1998). It consists of 2
159 concentric tubes with a heater and insulation around the outer tube. Sample air flows
160 through the inner tube, while water circulates between the inner and outer tubes. The
161 inner tube is made of porous extruded PTFE (polytetrafluoroethylene) membrane,
162 whose pore size is large enough for water molecules, but too small for larger
163 molecules such as oxygen to cross. The flux of water vapor through the membrane is
164 controlled by regulating the electric current to the humidifier heater until the desired
165 RH is attained. The humidity scan was a one-hour cycle; RH was ramped from ~40 to
166 90% during the first half hour and in the reverse direction during the last half hour.

167 Besides the scattering measurement, particle number size distribution and aerosol
168 chemistry were also measured at the station. Particle number size distributions from 3
169 nm to 10 μm were measured by a twin differential mobility particle sizer (TDMPMS)
170 (Birmili et al., 1999) and an aerodynamic particle sizer (APS, model 3321, TSI Inc.).
171 The mass concentrations of sulfate, nitrate, ammonium, organic matter (OM) and
172 chloride (aerodynamic diameter less than 1 μm) were measured by an aerosol mass
173 spectrometer (AMS, Aerodyne Inc.). The equivalent mass concentration of black
174 carbon (EBC) was measured by a multi angle absorption photometer (MAAP, mode
175 5012, Thermo Scientific Inc.) at [670–637](#) nm wavelength ([Müller et al., 2011](#)), the
176 assumed mass absorption cross-section was $6.6 \text{ m}^2 \text{ g}^{-1}$. Visibility was measured using
177 a near-forward scattering sensor (FD12, Vaisala). Meteorological data were provided
178 by the LinAn Regional Atmosphere Background Station.

179 All the instruments were housed in a measurement laboratory where room

180 temperature was controlled at ~25 °C. All data were reported in Beijing Time
181 (BJT=UTC+8 h) and all the scattering data were referenced at T=0 °C and P=1013.25
182 hPa. Truncation error correction, proposed by Anderson and Ogren in 1998 (Anderson
183 and Ogren, 1998), was applied to retrieve the final scattering and backscattering
184 coefficients. ~~The hemispheric backscatter fraction (b) was derived from equation~~
185 ~~$b = \sigma_{\text{bsp}} / \sigma_{\text{sp}}$ as mentioned above.~~ The Ångström exponent \mathring{a} was defined as
186 $\mathring{a} = -\log[\sigma_{\text{sp}}(\lambda_1) / \sigma_{\text{sp}}(\lambda_2)] / \log[\lambda_1 / \lambda_2]$. It represented the wavelength dependence of light
187 scattering assuming a power law relationship of σ_{sp} and σ_{bsp} . In this study, scattering
188 coefficients at 450 nm and 700 nm were used to derive \mathring{a} . Normalization of f(RH)
189 (Day and Malm, 2001) has been carried out to get the final f(RH) scan values, i.e.
190 f(40%) (the lowest RH in one cycle) is set to 1 and used to normalize other f(RH)
191 values in this cycle. It's worth mentioning that the normalization of f(RH) (see Sect.
192 2.2) may underestimate f(RH) to some extent, since some organics (e.g. humic acid
193 sodium) take up water even when RH <40% (Sjogren et al., 2007; Dick et al., 2000).
194 To evaluate its impact, we calculated the ~~unnormalized raw~~ f(40%) value without the
195 normalization the raw data. The average and standard deviation were 1.03 and 0.03
196 with a maximum of 1.08, which means this normalization may cause an underestimate
197 of 5% (an error of 3% was caused by the inconsistency of DryNeph and WetNeph,
198 see Sect. 2.4) at most. Figure 2c shows the un-normalized f(RH) value, the lowest
199 value of each cycle was around 1.03, considering the inconsistency of DryNeph and
200 WetNeph, f(RH) is close to unity at the lowest RH (~40%).

201 2.3 Inlet system

202 An automatic regenerating adsorption aerosol dryer (Tuch et al., 2009) was used
203 to provide low RH sample air to DryNeph, TDMPS, APS, AMS and MAAP to ensure
204 comparability of measurements. The aerosol dryer was housed in a separate shelter
205 which was located on the rooftop (~ 5 m a.g.l.) of the measurement laboratory.
206 Aerosols entered the shelter through a commercially available PM₁₀ impactor (PM₁₀
207 inlet, URG Corporation). Then these particles went through the adsorption aerosol
208 dryer (Tuch et al., 2009) to ensure the RH less than 30%. The dried aerosols passed
209 through a splitter via 3/4" stainless steel tubes, and then reached different instruments.

210 The total sample flow through this dryer inlet was kept at 16.7 lpm to ensure a 50%
211 collection efficiency at 10 μm aerodynamic diameter (Berner et al., 1979). Since a lot
212 of instruments share the total flow, the sample flow for the ~~Nephelometer~~
213 nephelometer is 9 lpm.

214 2.4 Quality control on scattering measurements

215 Accurate performance of nephelometers and RH sensors is crucial to retrieve
216 reliable enhancement factors ($f(\text{RH},\lambda)$, $f_b(\text{RH},\lambda)$ and $f_\beta(\text{RH},\lambda)$), since they are defined
217 as the ratio of aerosol scattering coefficient/ backscattering coefficient/ hemispheric
218 backscatter fraction at a higher RH to those at a low RH (usually $<34\%$). In addition,
219 the RH control in the WetNeph sensing volume is also critical to $f(\text{RH})$ measurement.
220 Therefore, several comparisons and calibrations have been carried out before and
221 during the experiment. Three external RH sensors (Vaisala, model HMP60) were
222 calibrated in the RH range of 11% to 80% using Vaisala Humidity Calibrator
223 (HMK15) with four saturated salt solutions (LiCl, K_2CO_3 , NaCl, $(\text{NH}_4)_2\text{SO}_4$), and
224 humidity/temperature transmitter (Vaisala, model HMT333), which was calibrated by
225 the National Center for Meteorological Metrology, China. Two internal ~~Nephelometer~~
226 nephelometer RH sensors were calibrated to the external RH sensors with an
227 uncertainty of $<2\%$. ~~Good~~ A good agreement of these RH sensors ~~were~~ was achieved
228 with the discrepancy $<3\%$. Both nephelometers were calibrated with CO_2 (purity
229 99.999%) and filtered air. Filtered air measurements were made automatically every
230 hour to track the instrument stability. Comparison of scattering and backscattering
231 coefficients of the two nephelometers under low RH (~~$<30\%$~~ $9.6 \pm 3.2\%$) was performed
232 during 1 to 3 March, 2013 (as shown in Fig. 2). The total scattering coefficient and
233 backscattering coefficient measured by WetNeph were, ~~on average,~~ constantly 3%
234 ($y=1.03x+1.60$, $R^2=1.000$) and 4% ($y=1.04x+0.09$, $R^2=0.997$) higher than those
235 obtained by DryNeph at 550 nm (similarly for other wavelengths), the high
236 consistency ~~which~~ demonstrates that the two nephelometers were operating quite
237 steadily and the scattering/backscattering coefficients measured by DryNeph can be
238 corrected in order to make them comparable to the measurements of WetNeph ~~within~~
239 their normal accuracy range. The uncertainty of nephelometer measurements was $\sim 10\%$

(Anderson et al, 1996), combining the uncertainty of the measurements of the internal RH sensor, the uncertainty of $f(85\%)$ was $\sim 20\%$ at large, which may decrease for less hygroscopic particles or smaller RHs.

The RH at the outlet of WetNeph was regulated via a feedback system between the Vaisala RH signal, a PID controller and a heater. The humidifier set point was stepped from low to high RH and back to low RH every hour with the set point changing every one or two minutes. Figure 3-2 is an example of our data showing the relative humidity control and corresponding scattering measurements. As can be seen from Fig. 32, good relative humidity control was achieved no matter whether the scattering/backscattering coefficient was high or low.

The nephelometers were operated at a constant flow of 20 lpm, comprised of 9 lpm sample air and 11 lpm particle-free air (dilution flow). The total flowrate through the nephelometer was controlled by a mass flow controller. The dilution flow was regulated by a needle valve and measured by a mass flowmeter. The sample and dilution flow have been calibrated with a Gilibrator bubble flowmeter before the experiment. Filtered air tests have also been conducted to make sure that all the instruments were in good condition and that there were no leaks in the system.

3 Results and discussion

3.1 Overview

Figure 3 shows the time series of the measured and derived aerosol variables in March 2013, as well as the ambient RH and visibility. The scattering enhancement factor $f(85\%)$ ranged from 1.29 to 1.86 (as shown in Fig. 4a3a) with an average of 1.58 (Table 1) for the whole campaign. During 4-9 March, $f(85\%)$ stayed at a low value of $1.42 (\pm 0.05)$ when LinAn was dominated by air masses from the south under clear sky. In March, the hourly averaged aerosol scattering coefficient under dry conditions (shown in Fig. 4e3c) varied from 21 to 1067 Mm^{-1} and the maximum occurred on 16 March, when a severe haze occurred. The mean value and standard deviation of the hourly averaged aerosol scattering coefficient was 223 Mm^{-1} (140 Mm^{-1}). Visibility (Fig. 4b3b) varied from 0.1 km to 23.7 km with a mean value of 6.2

270 km. It was quite low on 23 and 24 March because the station was in cloud. From 15 to
271 16 March, visibility declined to 4.4 km with the accumulation of pollutants in the
272 atmosphere, which was a severe haze episode (as mentioned above). An air mass from
273 Northwest China with high dust levels arrived at LinAn on 10 March, with an abrupt
274 increase of the aerosol scattering coefficient (Fig. 4e3c) and a sharp decline of
275 Ångström exponent (Fig. 4d3d).

276 Based on nephelometer measurements, the enhancement factors for scattering
277 coefficient $f(\text{RH})$, backscattering coefficient $f_b(\text{RH})$ and hemispheric backscatter
278 fraction $f_\beta(\text{RH})$ were determined by Eq. (1), (2) and (3), respectively. As can be seen
279 from Table 1, their values at different RHs (50, 60, 70, 80 and 85%) were obtained
280 using linear interpolation from the half-hourly humidogram data. The enhancement
281 factors $f(\text{RH})$ and $f_b(\text{RH})$ increased as the RH increased, but $f_b(\text{RH})$ increased much
282 more slowly than $f(\text{RH})$. The $f(85\%)$ and $f_b(85\%)$ were 1.58 and 1.25, respectively,
283 suggesting that the scattering coefficient and backscattering coefficient at 85% RH
284 were 58 and 25% higher than those in dry conditions due to aerosol water uptake. The
285 $f_\beta(\text{RH})$ decreased with increasing RH, i.e. hemispheric backscatter fraction becomes
286 smaller with the increase of RH and the fraction of radiation that would be
287 backscattered into space was reduced. The $f_\beta(\text{RH})$ decreased $\sim 21\%$ as the RH
288 increased from 40 to 85%. All these parameters are of crucial importance in
289 evaluating the aerosol radiative forcing.

290 Generally, the scattering enhancement factor ($f(80\%)=1.44$) is much lower than
291 the result ($f(80\%)=1.7-2.1$) obtained by Xu et al. (2002) for LinAn in 1999. This value
292 is also lower than the results obtained by Carrico during ACE-1 (Carrico et al., 1998)
293 and ACE-Asia (Carrico et al., 2003), the values obtained by Zieger et al. (2013) in
294 several European sites and the Arctic, as well as the values achieved by Malm and
295 Day (Malm et al., 2005; Malm et al., 2003; Malm and Day, 2001; Day and Malm,
296 2001; Malm and Day, 2000) in America. However, the difference between measured
297 $f(\text{RH})$ in this study and previous studies performed in China (Yan et al., 2009; Pan et
298 al., 2009; Liu et al., 2009; Delene and Ogren, 2002; Cheng et al., 2008) are much
299 smaller. The enhancement factor for backscattering coefficient and hemispheric

300 backscatter fraction ($f_b(85\%)$ and $f_\beta(85\%)$) is 1.25(0.07) and 0.79(0.04), respectively,
301 similar to the results ($f_b(82\%)=1.22\pm0.06$ and $f_\beta(82\%)=0.83$) obtained by Carrico at
302 Sagres, Portugal during ACE-2 (Carrico et al., 2000) and the results ($f_b(82\%)=1.27$
303 and $f_\beta(82\%)=0.75$) obtained by Carrico et al. (2003) during the dust-dominant period
304 in ACE-Asia.

305 **3.2 Aerosol chemical properties**

306 The submicron mass concentration of sulfate, nitrate, ammonium, chloride and
307 organic matter (OM) measured by AMS and EBC in PM_{10} measured by MAAP are
308 summarized in Table 2. The mass concentration of OM is the largest, while the mass
309 concentration of chloride is the smallest, in accord with previous studies in LinAn
310 (Meng et al., 2012; Yan et al., 2005). The mean mass concentration of nitrate and
311 sulfate were $9.8\pm12.1 \mu\text{g}\cdot\text{m}^{-3}$ and $8.1\pm4.1 \mu\text{g}\cdot\text{m}^{-3}$ in this study, similar to the values
312 ($9.4\pm7.1 \mu\text{g}\cdot\text{m}^{-3}$ for nitrate and $8.6\pm3.7 \mu\text{g}\cdot\text{m}^{-3}$ for sulfate in $PM_{2.5}$) at LinAn in 2010
313 summer (Meng et al., 2012).

314 Aerosol acidity is a key parameter affecting aerosol hygroscopic growth. It is
315 usually examined by comparing the NH_4^+ mass concentration measured by AMS and
316 the amount needed to fully neutralize sulfate, nitrate and chloride ions ($\text{NH}_4^+_{\text{predicted}}$)
317 (Sun et al., 2010):

$$318 \quad \text{NH}_4^+_{\text{predicted}} = 18 \times (2 * \text{SO}_4^{2-} / 96 + \text{NO}_3^- / 62 + \text{Cl}^- / 35.5) \quad (4)$$

319 Figure 5-4 illustrates the relationship of measured NH_4^+ and predicted NH_4^+ . As
320 shown in Fig. 5-4, the regression slope is close to 1, which implies that there was
321 sufficient NH_3 in the atmosphere to neutralize H_2SO_4 , HNO_3 and HCl , and that the
322 PM_1 aerosol at LinAn was bulk neutralized during the measurement period. Therefore,
323 the dominant chemical form of sulfate aerosol is ammonium sulfate (AS) rather than
324 acidic sulfate (H_2SO_4 or NH_4HSO_4) and the nitrate existed in the form of NH_4NO_3
325 (AN). By calculating Pearson's correlation coefficient among 5 different chemical
326 compositions, it could be found that NH_4^+ and NO_3^- are strongly correlated with
327 $r=0.93$; NH_4^+ and SO_4^{2-} , Cl^- are highly related with r equal to 0.77 and 0.74
328 respectively, which also implies the main form of inorganics would be NH_4NO_3 ,

329 (NH₄)₂SO₄ and NH₄Cl. However, because the average mass concentration of chloride
330 was very low (see Table 2) at LinAn, it suggests that NH₄NO₃ and (NH₄)₂SO₄ are the
331 dominant water-soluble ionic species, which are consistent with previous results at
332 LinAn based on filter chemical measurements (Meng et al., 2012).

333 **3.3 Wavelength dependence of the scattering enhancement factor f(85%)**

334 The wavelength dependence of scattering enhancement factor is needed to
335 estimate the aerosol radiative forcing since solar radiation at Earth's surface depends
336 on wavelength. The histograms for f(85%,550 nm), ~~f(85%,550 nm) f(85%,450 nm)~~
337 ~~and f(85%,550 nm) f(85%,700 nm) are~~ is shown in Fig. ~~65~~. Overlaid on the histogram
338 for f(85%,550 nm) (Fig. ~~6a5~~) are Gaussian curves based on the statistics for f(85%) at
339 each wavelength. No apparent shift of mean f(85%) is seen for the 550 nm and 700
340 nm wavelength pair (see Fig. ~~6a5 and Fig. 6e~~); while the mean f(85%,450 nm) is ~6%
341 lower than that at 550 nm with a smaller standard deviation (see Fig. ~~6a5 and Fig. 6b~~).
342 For higher values (90th and 70th percentile values in Table 3), slightly wavelength
343 dependence of f(RH) can be observed, i.e. the f(RH) increases with the increase of
344 wavelength. However, the differences are mostly under 10% (~~see Fig. 6b and Fig. 6e~~)
345 and therefore the discussion is focused on 550 nm wavelength in this study. Similar
346 results were obtained by Zieger at a regional continental research site at Melpitz,
347 Germany (Zieger et al., 2014).

348 **3.4 Classification of various observation episodes**

349 Based on wind direction, back trajectory analysis and weather phenomenon,
350 observation periods can be classified into three main sectors: a northerly-polluted
351 period (influenced by long-distance transport from northern China), a locally-polluted
352 period, and a dust-influenced episode. Air mass back trajectories over 72 hours at
353 300m a.g.l. arrival height were calculated using the Trajectory Statistics (TrajStat)
354 model (Wang et al., 2009) with 6-hourly archived meteorological data provided by the
355 US National Centers for Environmental Prediction (NCEP). The characteristics of
356 these three periods are as follows:

357 1. Periods when the wind direction is between 120 and 270 ° are chosen as
358 “locally-polluted periods”. During this period, pollutants mostly came from Anhui

359 province, Jiangxi province and the southern region of Zhejiang province as well as
360 LinAn (green line in Fig. 76). Economy in these areas is mainly made up of
361 manufacturing, tourism and agriculture.

362 2. Periods when the wind direction is greater than 270 or less than 120 ° are
363 described as “northerly-polluted periods”. Back trajectories indicate that most of
364 the air masses came from northern China and passed over heavily polluted areas
365 such as the Beijing-Tianjin-Tangshan economic region and the Yangtze River
366 Delta during long-distance transport (red line in Fig. 76).

367 3. A heavy dust event occurred at LinAn on 10 March (approximately from 02:00
368 BJT) according to satellite information (<https://earthdata.nasa.gov/labs/worldview/>)
369 and ~~3-h~~ meteorology information (provided by China Meteorological
370 Administration, CMA). The 72 h back trajectory shows the air masses tracked
371 from Mongolia and passed over Inner Mongolia (blue line in Fig. 76).

372 3.4.1 Locally-polluted period

373 In the periods of 4-9, 15-20 and 26-30 March, 2013 aerosols were mainly from
374 locally mixed pollutants from Zhejiang and/or nearby provinces. The mean $f(80\%)$
375 and $f(85\%)$ were 1.36 and 1.52 (as shown in Table 4), ~10 and 8% lower than those in
376 northerly-polluted periods.

377 The enhancement factor for scattering coefficient and backscattering coefficients
378 at 80% during locally-polluted period is 1.36 and 1.15, respectively, similar to the
379 values ($f(82.5\%)=1.4-1.5$) and ($f_{\beta}(82.5\%)=1.1-1.2$) obtained by Koloutsou-Vakakis et
380 al. (2001) at a northern hemisphere, continental site (Bondville, Illinois, US). The
381 measured dry scattering coefficient is 217 Mm^{-1} , ~15% lower than that of the
382 northerly-polluted period (251 Mm^{-1}). The averaged mass percentage of sulfate,
383 nitrate, ammonium, OM, chloride and EBC are 17.6, 16.1, 13.0, 42.2, 1.5 and 9.6%,
384 respectively (shown in Fig. 7a6a). Compared to the northerly-polluted period, the
385 mass percentage of OM is ~27% higher during the locally-polluted period, while the
386 mass percentage of nitrate is ~33% lower. Although the $\text{OM}/(\text{OM}+\text{SO}_4^{2-})$ ratios during
387 locally-polluted period (~0.70) and northerly-polluted period (~0.67) are similar, the
388 $\text{OM}/(\text{OM}+\text{NO}_3^-+\text{SO}_4^{2-})$ ratio during locally-polluted period (~0.56) is 24% higher

389 than that during northerly-polluted period (~0.45), which may partly explain the lower
390 f(RH) during locally-polluted episode (as discussed later in Sect. 3.5).

391 **3.4.2 Northerly-polluted period**

392 The air masses reaching LinAn during the period March 1-3, 11-15, 20-26 and
393 30-31 (dust episode excluded) mainly came from northern China through
394 long-distance transport. The mean f(80%) and f(85%) were 1.50 and 1.64 ,
395 respectively (as shown in Table 4).

396 The value (f(80%)=1.50) is similar to the previous results (f(80%)=1.48)
397 obtained by Yan et al. (2009) for periods under the downwind of urban plume from
398 Beijing, (f(80%)=1.46±0.10) reported by Carrico et al. (2000) for anthropogenic
399 aerosols in Europe during the 2nd Aerosol Characterization Experiment (ACE-2)
400 campaign, and (f(80%)=1.55-1.59) indicated by Pan et al. (2009) for a rural site
401 (Xin'an) near Beijing city during pollution periods. However, the measured f(80%)
402 was much lower than (f(80%)=2.0-2.43) during a pollution episode reported by Kim
403 et al. (2006) at the Gosan regional background site, 720 km northeast of LinAn and
404 results (f(82%)=2.24±0.20) obtained by Carrico et al. (2003) in ACE-Asia for polluted
405 air masses measured over the ocean. The f(RH) of continental air masses transported
406 over the ocean was higher than that over the continent, and the possible mechanisms
407 for that increase might include coagulation with sea-salt particles and the oxidation of
408 SO₂ and VOCs (volatile organic compounds) ~~to produce hygroscopic~~
409 ~~compounds~~ leading to an increase in the particle's hygroscopicity.

410 **3.4.3 Dust-influenced episode**

411 During a severe cold air outbreak, a strong dust event struck northern China
412 ~~experienced a strong dust event~~ on 8 and 9 March, 2013. The affected area covered
413 about 2.8 million square kilometers, about 0.27 million square kilometers of which
414 suffered from the dust storms or strong sandstorms ~~area covered about 0.27 million~~
415 ~~square kilometers, and. This event was~~ is considered to be the widest-largest and
416 strongest dust event to hit China in 2013. During this process, suspended dust
417 appeared in most of northwestern China, northern China, north and west Huanghuai
418 region and west Liaoning province, the west-central Inner Mongolia, west Gansu,

419 northern Shanxi, and several parts of Xinjiang experienced a sandstorm. Along with
420 the extreme dust event, there was a dramatic increase in PM₁₀, for example, the PM₁₀
421 in Yulin, Shanxi even reached 10,000 $\mu\text{g}\cdot\text{m}^{-3}$ (Wang et al., 2013;Zhang and Sun,
422 2013).

423 At 2 a.m. on March 10, wind direction changed abruptly to northerly (see Fig.
424 8d). The scattering coefficient increased abruptly from $\sim 200 \text{ Mm}^{-1}$ to $> 600 \text{ Mm}^{-1}$ (see
425 Fig. 8b7b). PM₁₀ mass concentrations at LinAn increased rapidly from 100 $\mu\text{g}\cdot\text{m}^{-3}$ to
426 637 $\mu\text{g}\cdot\text{m}^{-3}$, while the PM_{2.5} mass concentration was only 190 $\mu\text{g}\cdot\text{m}^{-3}$, accounting for
427 30% of PM₁₀. The Ångström exponent decreased from 1.2 to 0.8 (see Fig. 8e7c). All
428 these phenomena implied the arrival of cold front from northern China enriched in
429 coarse mode particles. The mass percentage of nitrate increased significantly and
430 reached its peak ($\sim 26\%$) at 3 a.m.; meanwhile, the mass percentage of OM decreased
431 sharply from 2 a.m. to 3 a.m. (see Fig. 8e7e). Correspondingly, the scattering
432 enhancement factor $f(85\%)$ reached 1.52 at 3 a.m. (see Fig. 8a7a), an increase of $\sim 16\%$
433 compared with that before the dust arrival. The most dust-dominated period, from 7
434 a.m. to 1 p.m., when the Ångström exponent was below 0.5 (Fig. 8e7c) and scattering
435 coefficients at 450 nm, 550 nm and 700 nm (Fig. 8b7b) were almost the same, the
436 scattering enhancement factor $f(85\%)$ was ~ 1.46 . This value is much higher than the
437 results ($f(80\%)=1.20$) reported by Pan et al. (2009) in rural Beijing, ($f(82.5\%)=1.18$)
438 obtained by Carrico et al. (2003) in East Asia (ACE-Asia) during a dust episode,
439 ($f(80\%)=1.20$) reported by Fierz-Schmidhauser et al. (2010) at a high alpine site
440 (Jungfrauoch, 3580m a.s.l.) in Switzerland during a strong Saharan dust event, and
441 ($f(80\%)=1.0-1.1$) measured by Li-Jones et al. (1998) in South America during an
442 investigation of long-range transported Saharan dust. Meanwhile it is much lower
443 than the value ($f(85\%)=1.73-2.20$) obtained by Kim et al. (2006) in Gosan (South
444 Korea) during a dust-dominated period. According to Tobo et al. (2010), Ca-rich
445 particles can react with gaseous HNO₃ to form Ca(NO₃)₂, thus the liquid
446 cloud-nucleating ability would be enhanced. Similar results have also reported that
447 aerosol hygroscopicity would be largely enhanced if coarse mode Ca-rich particles
448 combined with nitrate (Shi et al., 2008;Sullivan et al., 2009). Thus, it is speculated

449 that the relatively high $f(\text{RH})$ may have resulted from the reactions of coarse mode
450 particles with inorganics (very likely to be nitrate) during long-range transport.

451 **3.5 The relationship of scattering enhancement factor with chemical** 452 **compositions**

453 Scattering enhancement factor $f(85\%)$ versus organic mass fraction and inorganic
454 mass fraction were shown in Fig. 98. The total mass concentration was calculated as
455 the sum of mass concentrations of sulfate, nitrate, ammonium, chloride and organic
456 measured by AMS and EBC measured by MAAP. The organic and inorganic mass
457 fractions were calculated by dividing the mass concentration of organics (measured
458 by AMS) and inorganics (the sum of sulfate, nitrate, ammonium and chloride
459 measured by AMS) by the total mass concentration, respectively. The bivariate linear
460 regression was applied with the uncertainty of $f(85\%, 550\text{nm})$ which was discussed in
461 Sect. 2.4 and the standard deviation of chemical compositions. ~~As~~ The bivariate
462 linear regressions shown in (Fig. 98) show clearly anti-correlation of $f(85\%, 550\text{nm})$
463 to organics fraction and strongly positive correlation of $f(85\%, 550\text{nm})$ to inorganics
464 fraction, organics were clearly anti-correlated to $f(85\%)$, while inorganics showed
465 strongly positive correlation with $f(85\%)$ ($R^2=0.86$). This implies that chemical
466 composition plays a vital role in aerosol hygroscopic properties. The absolute values
467 of both slopes (~~1.11, 2~~ for $f(85\%)$ vs. organic mass fraction and 0.96 for $f(85\%)$ vs.
468 inorganic mass fraction) were much lower than those (3.1 and 2.2, respectively)
469 measured at Melpitz, Germany (Zieger et al., 2014). This may partly account to the
470 higher organic (or lower inorganic) contents at LinAn. Comparing Fig. 9-8 (a)(b) and
471 (c)(d), a more clearly trend of increasing nitrate with increasing $f(85\%)$ was observed.
472 The role nitrate plays in aerosol hygroscopic properties will be discussed in the
473 following paragraph.

474 $f(\text{RH})$ in Fig. 10-9 was expressed in terms of γ so as to be applied to a broader
475 RH range (Doherty et al., 2005; Quinn et al., 2005):
476 $\gamma = \ln f(\text{RH}) / \ln((100 - \text{RH}_{\text{ref}}) / (100 - \text{RH}))$. Here γ was based on $\text{RH}_{\text{ref}} = 40\%$ and $\text{RH} = 85\%$.
477 The relative amount of OM and inorganics can be expressed as $F_o = C_c / (C_c + C_i)$, where
478 C_c and C_i are the mass concentrations of OM and inorganics, respectively. Figure 10-9

479 shows γ versus F_o where C_i was the mass concentrations of SO_4^{2-} , NO_3^- and
480 $NO_3^-+SO_4^{2-}$ in Fig. [10a9a](#), Fig. [10b9b](#) and Fig. [10e9c](#), respectively. For all the three
481 scatter plots, there is a trend of decreasing γ with increasing F_o . However, unlike the
482 results of Quinn et al. (2005), Malm et al. (2005), Pan et al. (2009) and Yan et al.
483 (2009), γ and F_o ($OM/(OM+SO_4^{2-})$) (shown in Fig. [10a9a](#)) were uncorrelated
484 ($R^2=0.14$), while γ and F_o ($OM/(OM+NO_3^-)$) (shown in Fig. [10b9b](#)) and γ and F_o
485 ($OM/(OM+SO_4^{2-}+NO_3^-)$) (shown in Fig. [10e9c](#)) were more strongly correlated (R^2 of
486 0.56 and 0.68, respectively). This result implies that NO_3^- (rather than SO_4^{2-}) plays
487 an important role in aerosol hygroscopic growth during this study.. This increasingly
488 importance of nitrate corresponds to many recent studies in Shanghai (a mega city in
489 Yangtze River Delta) (Shi et al., 2014) and Beijing (Sun et al., 2012). This may partly
490 result from increasing availability of NH_3 to form NH_4NO_3 (Morgan et al., 2010) due
491 to the decrease of SO_2 . Chinese government has put an emphasis on the control of
492 SO_2 emission in recent years. The desulfurization technology were installed at
493 coal-fired power units as well as certain steel and cement production facilities, as a
494 result, the annual average concentration of SO_2 decreased significantly from 56 to 19
495 $\mu g m^{-3}$ at LinAn from 2006 to 2012 (ZEPB, 2012; 2006).

496 The molar ratio of particulate SO_4^{2-} to total sulfur ($SO_4^{2-}+gas\ phase\ SO_2$) was
497 used as an indicator of the relative age of aerosols (Quinn et al., 2005). For relatively
498 younger aerosols, there is insufficient time for the conversion of SO_2 to SO_4^{2-} via gas
499 and aqueous phase oxidation process and therefore the $SO_4^{2-}/(SO_4^{2-}+SO_2)$ molar ratio
500 is low. As aerosol ages, more SO_2 is converted to SO_4^{2-} and thus the ratio increases.
501 To illustrate the effects of this ratio and scattering coefficient on γ , Fig. [11-10](#) shows γ
502 versus $F_o=OM/(OM+SO_4^{2-}+NO_3^-)$ colored by the $SO_4^{2-}/(SO_4^{2-}+SO_2)$ molar ratio (Fig.
503 [11a10a](#)) and $\log_{10}(\sigma_{sp})$ (Fig. [11b10b](#)). The highest values of γ (or $f(RH)$)
504 corresponded to more aged aerosols with a low OM content ; while the lowest values
505 corresponded to younger aerosols with a higher OM content, consistent with the result
506 of Quinn et al. (2005). For aerosols with relatively low scattering coefficient, the
507 value of $f(RH)$ was usually low with a large variation (dots with cooler colors in Fig.
508 [11b10b](#)); while aerosols with high scattering coefficients, the value of $f(RH)$ was

509 | relatively high with a small variation(dots with warm colors in Fig. [4b10b](#)).

510 **3.6 Parameterization of scattering enhancement factor f(RH)**

511 Scattering enhancement factor f(RH) can be parameterized using empirical
512 equations (Kotchenruther and Hobbs, 1998; Kotchenruther et al., 1999; Gass ó et al.,
513 2000; Carrico et al., 2003; Liu et al., 2008; Pan et al., 2009; Zieger et al., 2010; Zieger
514 et al., 2014). Humidograms of LinAn were fitted into two empirical equations and the
515 fitting results were shown below.

516 **3.6.1 Parameterization with equation $f(\text{RH})=c (1-\text{RH})^{-g}$**

517 Kasten (1969) proposed an empirical equation $f(\text{RH})=c (1-\text{RH})^{-g}$ to describe how
518 f(RH) varies with RH, which has been used in previous reports e.g. by Kotchenruther
519 and Hobbs (1998), Gass ó et al. (2000), Carrico et al. (2003) and Zieger et al. (2010,
520 2014). Table 5 shows the fitting results of this work and other previous studies. The
521 larger “c” and “g”, the larger f(RH). In this work, “g” was much lower than that in
522 most of the other studies, while was similar to the result of Gass ó et al. (2000) during
523 dust episode. It results from the comparably low scattering enhancement factor (e.g.
524 $f(80\%)=1.44\pm 0.12$) of LinAn, which was similar to the value ($f(80\%)=1.33\pm 0.07$)
525 obtained by Gass ó et al. (2000) for a dust event. The f(RH) in other studies was much
526 higher than that at LinAn, ranging from 2.04 (polluted marine aerosols in Gass ó et al.
527 (2000)) to 3.77 (arctic aerosols in Zieger et al. (2010)), therefore their parameter “g”
528 was much higher.

529 **3.6.2 Parameterization with equation $f(\text{RH})=1+a \text{RH}^b$**

530 The f(RH) obtained at LinAn station can be well described by the following
531 equation, which was proposed by Kotchenruther and Hobbs (1998):

$$532 \quad f(\text{RH})=1+a \text{RH}^b \quad (5)$$

533 where “a” is positive and “b” is greater than 1. This function is convex, and has been
534 used in many previous studies (Pan et al., 2009;Delene and Ogren, 2002;Carrico et al.,
535 2003;Kotchenruther et al., 1999;Kotchenruther and Hobbs, 1998) to describe
536 monotonic growth. Theoretically, parameter “a” determines the largest value f(100%)
537 can reach, and parameter “b” dominates the curvature of the function. The smaller “b”
538 is, the smaller the curvature of humidogram will be; if “b” equals to 1, then

539 $f(\text{RH})=1+a\cdot\text{RH}$. The parameters “a” and “b” from our study and previous results for
540 different aerosol types are listed in Table 6. Taking the locally-polluted episode as an
541 example, although parameter “a” is slightly larger (~3%) than in northerly-polluted
542 episode, parameter “b” is ~40% ~~greater~~larger, as a result the $f(85\%)$ during
543 locally-polluted period is smaller. Parameter “b” is the largest in the locally-polluted
544 episode, and smallest in the northerly-polluted period, i.e. the curvature of $\text{RH}-f(\text{RH})$
545 line is largest during the locally-polluted episode, then is the dust episode, and
546 northerly-polluted period is the smallest, which is consistent with the mass
547 percentages of nitrate (see Fig. [76](#)) (will be discussed later).

548 3.6.3 Steepness of humidograms

549 Among all the humidograms measured at LinAn, $f(\text{RH})$ increases continuously
550 and monotonically. However, the curvatures of ~~the different~~ humidograms are
551 different (Fig. [1211](#)): some increase with a nearly constant rate and the humidogram
552 line is almost straight, while some increase slowly at first and then increase more
553 steeply at relatively higher RH, thus the curvature of the humidogram is ~~greater~~larger.
554 In order to describe the growth pattern quantitatively, a steepness index η is defined
555 based on the fitting curve:

$$556 \quad \eta=f'(80\%)/f'(60\%)-1=(4/3)^{b-1}-1 \quad (6)$$

557 where $f'(60\%)$ and $f'(80\%)$ represent the derivatives of the fitting curve at 60% and 80%
558 RH, respectively. η is a nonnegative number. Zieger et al. (2010) has defined an index
559 describing the magnitude of deliquescence transitions based on fitting equation
560 $f(\text{RH})=(1-\text{RH})^{-\eta}$ (see Sect. 3.6.1), while the steepness index η proposed in this study
561 provided a way of quantitatively describing the steepness of humidograms well fitted
562 into equation $f(\text{RH})=1+a\text{RH}^b$. The ~~bigger-larger~~ η is, the ~~greater-bigger~~ the curvature.
563 As is shown in Fig. [12a11a](#), for a large η , the $f(60\%)$ is very small, meaning that
564 aerosol scattering coefficient barely increases ($f(\text{RH})\approx 1$) under low RH (usually
565 $<70\%$). Once reaching larger RH (~70%), $f(\text{RH})$ begins to increase. However, for a
566 small η (Fig. [12b11b](#)), the difference of the derivatives at 60% and 80% RH was small,
567 meaning the curvature of humidogram is much smaller.

568 A scatter plot of η and the mass percentage of nitrate is shown in Fig. [1312](#),

569 colored by the mass percentage of sulfate. As can be seen, η is negatively correlated
 570 with the mass percentage of nitrate. When the mass percentage of nitrate is below
 571 $\sim 18\%$, the more nitrate, the smaller η is, which means the humidogram line becomes
 572 straighter and the difference of the derivatives at lower and higher RHs becomes
 573 smaller. For a mass percentage of nitrate higher than 18% (correspondingly, a lower
 574 sulfate mass percentage), η is ~ 1.1 , meaning the humidogram line is almost straight
 575 (as shown in Fig. [42b11b](#)) and aerosol scattering coefficient experiences a continuous
 576 and smooth growth at almost the same rate with RH.

577 3.7 Sensitivity of the direct radiative forcing of different aerosols to $f(\text{RH})$

578 Direct radiative forcing of aerosols is quite sensitive to changes of relative
 579 humidity. The impact of relative humidity on globally-averaged, direct radiative
 580 forcing can be obtained by the following expression (Chylek and Wong, 1995):

$$581 \quad \Delta F_R(\text{RH}) = -[S_0/4][T_a^2(1 - A_c)][2(1 - R_s)^2\bar{\beta}(\text{RH})M\alpha_s f(\text{RH}) - 4R_s M\alpha_a] \quad (7)$$

582 where S_0 is the solar constant, T_a is the transmittance of the atmosphere above the
 583 aerosol layer, A_c is the fractional cloud amount, R_s is the albedo of the underlying
 584 surface, $\bar{\beta}(\text{RH})$ is the solar radiation scattered back to space at defined RH, $f(\text{RH})$ is
 585 the scattering enhancement factor, M is the column burden of aerosol (in g m^{-2}), α_s is
 586 the mass scattering efficiency, and α_a is the mass absorption efficiency.

587 In order to estimate the sensitivity of the forcing to ~~the observed values of~~
 588 $f(\text{RH})$ different RHs for various aerosol types (locally-polluted, northerly-polluted
 589 and dust-influenced aerosols), the ratio of direct aerosol radiative forcing ΔF_R at a
 590 defined RH to that at dry condition was calculated:

$$\frac{\Delta F_R(\text{RH})}{\Delta F_R(\text{dry})} = \frac{(1 - R_s)^2\bar{\beta}(\text{RH})\alpha_s f(\text{RH}) - 2R_s\alpha_a}{(1 - R_s)^2\bar{\beta}(\text{dry})\alpha_s f(\text{dry}) - 2R_s\alpha_a} \quad (8)$$

591 Parameters used in Eq. (8) were $R_s=0.15$, and $\alpha_a=0.3 \text{ m}^2\cdot\text{g}^{-1}$ (Wang et al., 2012; Hand
 592 and Malm, 2007). The mass scattering efficiency α_s is $2.76 \text{ m}^2\cdot\text{g}^{-1}$, which is derived
 593 from the slope of a linear regression of the measured scattering coefficients and the
 594 calculated PM_{10} mass concentrations based on TDMPS and APS measurement (see
 595 Fig. [4413](#)); the high mass scattering efficiency is explained by the high ratio of PM_1 to
 596 PM_{10} mass at this site (average 0.81). The average upscatter fraction $\bar{\beta}$ was

597 calculated as $\bar{\beta}=0.0817+1.8495b-2.9682b^2$ (Delene and Ogren, 2002). The sensitivity
598 of direct radiative forcing to RH for various aerosol types were shown in Fig. 14. As
599 is shown in the figure, the variation of $\Delta F_R(\text{RH})/\Delta F_R(\text{dry})$ with RH was in accordance
600 with the variation of humidograms. The $f(\text{RH})$ was the largest during the
601 northerly-polluted period, correspondingly, the effects of RH on aerosol radiative
602 forcing during this period was the largest. The same was true for the locally-polluted
603 period and the dust-influenced period. Since b decreases with increasing RH, this
604 correspondence also demonstrated the vital role $f(\text{RH})$ played in direct forcing
605 enhancement. At 85% RH, the average ratio was 1.47, i.e. the direct radiative forcing
606 increased by 47% owing to the aerosol hygroscopicity.

607 Table 7 shows the mean influence of aerosol hygroscopicity on direct radiative
608 forcing in March at LinAn. The ratios $\Delta F_R(\text{RH}_{\text{amb}})/\Delta F_R(\text{dry})$ for locally-polluted,
609 northerly-polluted and dust-influenced aerosols ~~are were calculated~~ presented in
610 Table 7, where $\Delta F_R(\text{RH}_{\text{amb}})$ was calculated at using the ambient average ~~relative~~
611 ~~humidity~~ RH ($\text{RH}_{\text{amb}}=67\%$) in March at LinAn. The variables $f(\text{RH}_{\text{amb}})$, $b(\text{RH}_{\text{amb}})$,
612 $\bar{\beta}(\text{RH}_{\text{amb}})$ and $\Delta F_R(\text{RH}_{\text{amb}})/\Delta F_R(\text{dry})$ were the averages of the linear interpolation
613 results of $f(\text{RH})$, $b(\text{RH})$, $\bar{\beta}(\text{RH})$ and $\Delta F_R(\text{RH})/\Delta F_R(\text{dry})$ at 67% RH.

614 ~~As shown in Eq. (8), $f(\text{RH})$ has a direct influence on the ratios $\Delta F_R(\text{RH})/\Delta F_R(\text{dry})$.~~
615 ~~At the ambient average RH of 67%, the average $f(\text{RH}_{\text{amb}})$ s for locally polluted,~~
616 ~~northerly-polluted and dust-influenced aerosols were 1.17, 1.26 and 1.15, respectively,~~
617 ~~thus the~~ The ratios $\Delta F_R(\text{RH}_{\text{amb}})/\Delta F_R(\text{dry})$ ratios were 1.118, 1.195 and 1.105,
618 respectively (see Table 7). That is to say, averagely, the direct radiative forcing of
619 locally-polluted, northerly-polluted and dust-influenced aerosols increased by 11.8,
620 19.5 and 10.5% in March at LinAn. ~~due to the aerosol hygroscopic growth at~~
621 ~~RH=67%. We could also see that the $f(\text{RH})$ and the ratio $\Delta F_R(\text{RH})/\Delta F_R(\text{dry})$ for~~
622 ~~northerly-polluted aerosols were the largest, which suggests the effect of $f(\text{RH})$ on~~
623 ~~direct radiative forcing is larger than that of the upscatter fraction $\bar{\beta}(\text{RH})$, since $\bar{\beta}(\text{RH})$~~
624 ~~shows negative relationship with $f(\text{RH})$.~~

625

626 **4 Conclusions**

627 The influence of aerosol water uptake on particles' light scattering properties and
628 direct radiative forcing have been investigated at LinAn, a regional atmospheric
629 background station of Yangtze River Delta, China, using the scattering enhancement
630 factor measurement system, together with AMS, MAAP and TDMPS providing the
631 chemical composition and size distribution information. The average enhancement
632 factors and mean standard deviations at 85% RH for scattering coefficient,
633 backscattering coefficient and hemispheric backscatter fraction ($f(85\%)$, $f_b(85\%)$ and
634 $f_{\beta}(85\%)$) were 1.58(0.12), 1.25(0.07) and 0.79(0.04), respectively, ~~which means that~~
635 ~~at 85% RH, the aerosol scattering coefficient and backscattering coefficient increased~~
636 ~~by 58 and 25%. The mean values of $f(85\%)$ at 550nm and 700nm were similar; while~~
637 ~~the mean $f(85\%, 450\text{nm})$ was approx. 6% lower.~~ Slight wavelength dependence of
638 $f(85\%)$ was observed at higher $f(\text{RH})$ values.

639 ~~Our experimental data from LinAn station can be categorized into 3 episodes~~
640 ~~(northerly polluted, locally polluted and dust episodes) according to the wind~~
641 ~~direction, back trajectory and weather phenomenon. (1) During the locally polluted~~
642 ~~period, air masses mainly came from relatively clean districts, and the corresponding~~
643 ~~average and mean standard deviation of $f(85\%)$, $f_b(85\%)$ and $f_{\beta}(85\%)$ were 1.52(0.10),~~
644 ~~1.21(0.06) and 0.80(0.02), respectively; (2) During the northerly polluted period, air~~
645 ~~masses came from northern China and passed through heavily polluted areas, and the~~
646 ~~average and mean standard deviation of $f(85\%)$, $f_b(85\%)$ and $f_{\beta}(85\%)$ were 1.64(0.09),~~
647 ~~1.28(0.06) and 0.78(0.02), respectively; (3) The average and mean standard deviation~~
648 ~~of $f(85\%)$ during dust episode was 1.48(0.05), much higher than the values~~
649 ~~immediately before dust arrival.~~

650 Generally, the highest values of $f(\text{RH})$ corresponded to aged aerosols with a
651 small fraction of OM; while the lowest values corresponded to younger aerosols with
652 a larger fraction of OM. $f(\text{RH})$ of aerosols with relatively low scattering coefficient
653 was usually low with a large variation; while $f(\text{RH})$ of aerosols with high scattering
654 coefficients was relatively high with a small variation. ~~Unlike the results of many~~
655 ~~previous reports like Quinn et al. (2005), Malm et al. (2005), Pan et al. (2009) and~~

656 ~~Yan et al. (2009), $f(85\%)$ and $OM/(OM+SO_4^{2-})$ were unrelated in this study, while~~
657 ~~Besides,~~ NO_3^- plays an important role in determining the magnitude of $f(RH)$ at
658 LinAn.

659 ~~The hH humidograms measured at LinAn can be well described by the model~~
660 ~~$f(RH)=c(1-RH)^d$ and model $f(RH)=1+aRH^b$, and the “a” and “b” for each episode~~
661 ~~are: 1.24 ± 0.29 and 5.46 ± 1.90 for locally polluted period, 1.20 ± 0.21 and 3.90 ± 1.27 for~~
662 ~~northerly polluted period, and 1.02 ± 0.19 and 4.51 ± 0.80 for dust episode.~~ Further
663 investigation shows the shape of the humidogram is closely related to the mass
664 percentage of nitrate. A ~~variable steepness index~~ η has been defined to quantitatively
665 determine the ~~degree of the curvature steepness~~ of humidograms. The more nitrate (or
666 less sulfate), the smaller η is and the straighter the curve will be. ~~When mass~~
667 ~~percentage of nitrate is larger than 18%, most of η is approx. 1.1, which means the~~
668 ~~aerosol scattering increases continuously and monotonically with a nearly constant~~
669 ~~speed.~~

670 In March, the average relative humidity (RH_{amb}) was 67%. ~~and the averaged~~
671 ~~$f(RH_{amb})$ s for locally polluted, northerly polluted and dust influenced aerosols were~~
672 ~~1.17, 1.26 and 1.15, respectively. Correspondingly, Consequently, the direct~~
673 radiative forcing of locally-polluted, northerly-polluted and dust-influenced aerosols
674 increased by 11.8, 19.5 and 10.5%, respectively due to aerosol uptake water in March
675 at LinAn. At 85% RH, the direct radiative forcing increased by as high as 47% due to
676 the aerosol hygroscopicity. In conclusion, water plays an important role in aerosol
677 scattering properties as well as the radiative forcing, and it should be paid high
678 attention when comparing between remote sensing and in-situ measurements and
679 calculating the climate forcing.

680

681

682 **Acknowledgments:** This work was supported by National Basic Research Program of
683 China (2011CB403401), the National Natural Science Foundation of China
684 (41475118, 41175113), China International Science and Technology Cooperation
685 Project (2009DFA22800), CAMS Basis Research Project (2013Z007, 2013Y004),

686 and the Meteorological Special Project of China (GYHY-200906038,
687 GYHY201206037). [This paper is partially supported by the CMA Innovation Team](#)
688 [for Haze-fog Observation and Forecasts.](#) The authors would also like to thank the
689 LinAn observational station staff for their support. The authors would thank [Dr. D.](#)
690 [Covert of University of Washington Seattle Department of Atmospheric Sciences](#)
691 [USA](#) for useful discussions.

692

693

694 **References**

- 695 Ackerman, A. S., Kirkpatrick, M. P., Stevens, D. E., and Toon, O. B.: The impact of humidity above
696 stratiform clouds on indirect aerosol climate forcing, *Nature*, 432, 1014-1017, 2004.
- 697 Adam, M., Putaud, J., Martins dos Santos, S., Dell'Acqua, A., and Gruening, C.: Aerosol hygroscopicity
698 at a regional background site (Ispra) in Northern Italy, *Atmos. Chem. Phys*, 12, 5703-5717, 2012.
- 699 Anderson, T., Covert, D., Marshall, S., Laucks, M., Charlson, R., Waggoner, A., Ogren, J., Caldow, R.,
700 Holm, R., and Quant, F.: Performance characteristics of a high-sensitivity, three-wavelength, total
701 scatter/backscatter nephelometer, *J. Atmos. Ocean. Tech.*, 13, 967-986, 1996.
- 702 Anderson, T. L., and Ogren, J. A.: Determining aerosol radiative properties using the TSI 3563
703 integrating nephelometer, *Aerosol Sci. Tech.*, 29, 57-69, 1998.
- 704 Berner, A., Lürzer, C., Pohl, F., Preining, O., and Wagner, P.: The size distribution of the urban aerosol in
705 Vienna, *Sci. Total Environ.*, 13, 245-261, 1979.
- 706 Birmili, W., Stratmann, F., and Wiedensohler, A.: Design of a DMA-based size spectrometer for a large
707 particle size range and stable operation, *J. Aerosol Sci.*, 30, 549-553, 1999.
- 708 Carrico, C. M., Rood, M. J., and Ogren, J. A.: Aerosol light scattering properties at Cape Grim, Tasmania,
709 during the first Aerosol Characterization Experiment (ACE 1), *J. Geophys. Res.*, 103, 16565-16574,
710 1998.
- 711 Carrico, C. M., Rood, M. J., Ogren, J. A., Neusüß, C., Wiedensohler, A., and Heintzenberg, J.: Aerosol
712 Optical properties at Sagres, Portugal during ACE-2, *Tellus B*, 52, 694-715, 2000.
- 713 Carrico, C. M., Kus, P., Rood, M. J., Quinn, P. K., and Bates, T. S.: Mixtures of pollution, dust, sea salt,
714 and volcanic aerosol during ACE-Asia: Radiative properties as a function of relative humidity, *J.*
715 *Geophys. Res.*, 108, 8650, 10.1029/2003JD003405, 2003.
- 716 Charlson, R.J., Ahlquist, N., Selvidge, H., and MacCready Jr, P.: Monitoring of atmospheric aerosol
717 parameters with the integrating nephelometer, *JAPCA J. Air Waste Ma.*, 19, 937-942, 1969.
- 718 Charlson, R. J., Schwartz, S., Hales, J., Cess, R. D., Coakley Jr, J. A., Hansen, J., and Hofmann, D.: Climate
719 forcing by anthropogenic aerosols, *Science*, 255, 423-430, 1992.
- 720 Cheng, Y., Wiedensohler, A., Eichler, H., Heintzenberg, J., Tesche, M., Ansmann, A., Wendisch, M., Su,
721 H., Althausen, D., and Herrmann, H.: Relative humidity dependence of aerosol optical properties
722 and direct radiative forcing in the surface boundary layer at Xinken in Pearl River Delta of China: An
723 observation based numerical study, *Atmos. Environ.*, 42, 6373-6397, 2008.
- 724 Chylek, P., and Wong, J.: Effect of absorbing aerosols on global radiation budget, *Geophys. Res. Lett.*,
725 22, 929-931, 1995.

726 Covert, D. S., Charlson, R., and Ahlquist, N.: A study of the relationship of chemical composition and
727 humidity to light scattering by aerosols, *J. Appl. Meteorol.*, 11, 968-976, 1972.

728 Day, D. E., and Malm, W. C.: Aerosol light scattering measurements as a function of relative humidity: a
729 comparison between measurements made at three different sites, *Atmos. Environ.*, 35, 5169-5176,
730 2001.

731 Delene, D. J., and Ogren, J. A.: Variability of aerosol optical properties at four North American surface
732 monitoring sites, *J. Atmos. Sci.*, 59, 1135-1150, 2002.

733 Dick, W. D., Saxena, P., and McMurry, P. H.: Estimation of water uptake by organic compounds in
734 submicron aerosols measured during the Southeastern Aerosol and Visibility Study, *J. Geophys.*
735 *Res.-Atmos.*, 105, 1471-1479, 2000.

736 Doherty, S. J., Quinn, P. K., Jefferson, A., Carrico, C. M., Anderson, T. L., and Hegg, D.: A comparison and
737 summary of aerosol optical properties as observed in situ from aircraft, ship, and land during
738 ACE-Asia, *J. Geophys. Res.*, 110, D04201, doi: 10.1029/2004JD004964, 2005.

739 Engelhart, G., Hildebrandt, L., Kostenidou, E., Mihalopoulos, N., Donahue, N., and Pandis, S.: Water
740 content of aged aerosol, *Atmos. Chem. Phys.*, 11, 911-920, 2011.

741 Fang, S. X., Zhou, L. X., Masarie, K. A., Xu, L., and Rella, C. W.: Study of atmospheric CH₄ mole fractions
742 at three WMO/GAW stations in China, *J. Geophys. Res.-Atmos.*, 118, 4874-4886, 2013.

743 Fierz-Schmidhauser, R., Zieger, P., Gysel, M., Kammermann, L., DeCarlo, P., Baltensperger, U., and
744 Weingartner, E.: Measured and predicted aerosol light scattering enhancement factors at the high
745 alpine site Jungfraujoch, *Atmos. Chem. Phys.*, 10, 2319-2333, 2010.

746 [Gasso, S., Hegg, D., Covert, D., Collins, D., Noone, K., Öström, E., Schmid, B., Russell, P., Livingston, J.,
747 and Durkee, P.: Influence of humidity on the aerosol scattering coefficient and its effect on the
748 upwelling radiance during ACE-2, *Tellus B*, 52, 546-567, 2000.](#)

749 Hänel, G.: The properties of atmospheric aerosol particles as functions of the relative humidity at
750 thermodynamic equilibrium with the surrounding moist air, *Adv. Geophys.*, 19, 73-188, 1976.

751 Hand, J., and Malm, W.: Review of aerosol mass scattering efficiencies from ground-based
752 measurements since 1990, *J. Geophys. Res.-Atmos.*, 112, D16203, doi:10.1029/2007JD008484,
753 2007.

754 Kim, J., Yoon, S.-C., Jefferson, A., and Kim, S.-W.: Aerosol hygroscopic properties during Asian dust,
755 pollution, and biomass burning episodes at Gosan, Korea in April 2001, *Atmos. Environ.*, 40,
756 1550-1560, 2006.

757 Koloutsou-Vakakis, S., Carrico, C., Kus, P., Rood, M., Li, Z., Shrestha, R., Ogren, J., Chow, J., and Watson,
758 J.: Aerosol properties at a midlatitude Northern Hemisphere continental site, *J. Geophys. Res.*, 106,
759 3019-3032, 2001.

760 Kotchenruther, R. A. and Hobbs, P. V.: Humidification factors of aerosols from biomass burning in
761 Brazil, *J. Geophys. Res.*, 103, 32081-32089, doi: 10.1029/98jd00340, 1998.

762 Kotchenruther, R. A., Hobbs, P. V., and Hegg, D. A.: Humidification factors for atmospheric aerosols off
763 the mid-Atlantic coast of the United States, *J. Geophys. Res.*, 104, 2239-2251, 1999.

764 Li-Jones, X., Maring, H. B., and Prospero, J. M.: Effect of relative humidity on light scattering by mineral
765 dust aerosol as measured in the marine boundary layer over the tropical Atlantic Ocean, *J. Geophys.*
766 *Res.*, 103, 31113-31121, 1998.

767 Liu, X., Zhang, Y., Jung, J., Gu, J., Li, Y., Guo, S., Chang, S.-Y., Yue, D., Lin, P., Kim, Y. J., Hu, M., Zeng, L.,
768 and Zhu, T.: Research on the hygroscopic properties of aerosols by measurement and modeling
769 during CAREBeijing-2006, *J. Geophys. Res.-Atmos.*, 114, D00G16, doi: 10.1029/2008JD010805, 2009.

770 Magi, B. I., and Hobbs, P. V.: Effects of humidity on aerosols in southern Africa during the biomass
771 burning season, *J. Geophys. Res.-Atmos.* 108, 8504, doi:10.1029/2002JD002144, 2003.

772 Malm, W. C., and Day, D. E.: Optical properties of aerosols at Grand Canyon national park, *Atmos.*
773 *Environ.*, 34, 3373-3391, 2000.

774 Malm, W. C., and Day, D. E.: Estimates of aerosol species scattering characteristics as a function of
775 relative humidity, *Atmos. Environ.*, 35, 2845-2860, 2001.

776 Malm, W. C., Day, D. E., Kreidenweis, S. M., Collett, J. L., and Lee, T.: Humidity-dependent optical
777 properties of fine particles during the Big Bend Regional Aerosol and Visibility Observational Study, *J.*
778 *Geophys. Res.*, 108, 4279, doi:10.1029/2002JD002998, 2003.

779 Malm, W. C., Day, D. E., Kreidenweis, S. M., Collett, J. L., Carrico, C., McMeeking, G., and Lee, T.:
780 Hygroscopic properties of an organic-laden aerosol, *Atmos. Environ.*, 39, 4969-4982, 2005.

781 Meng, Z. Y., Jia, X. F., Zhang, R. J., Yu, X. M., and Ma, Q. L.: Characteristics of PM_{2.5} at Lin'an Regional
782 Background Station in the Yangtze River Delta Region, *J. Appl. Meteorol. Sci.*, 23, 424-432, 2012.

783 Morgan, W., Allan, J., Bower, K., Esselborn, M., Harris, B., Henzing, J., Highwood, E., Kiendler-Scharr, A.,
784 McMeeking, G., and Mensah, A.: Enhancement of the aerosol direct radiative effect by
785 semi-volatile aerosol components: airborne measurements in North-Western Europe, *Atmos. Chem.*
786 *Phys.*, 10, 8151-8171, 2010.

787 [Müller T., Laborde M., Kassell G., and Wiedensohler A., Design and performance of a three wavelength](#)
788 [LED-based total scatter and backscatter integrating nephelometer, *Atmos. Meas. Tech.*, 4\(6\), 1291-](#)
789 [1303, doi:10.5194/amt-4-1291-2011, 2011.](#)

790 Pan, L., Che, H., Geng, F., Xia, X., Wang, Y., Zhu, C., Chen, M., Gao, W., and Guo, J.: Aerosol optical
791 properties based on ground measurements over the Chinese Yangtze Delta Region, *Atmos. Environ.*,
792 44, 2587-2596, 2010.

793 Pan, X. L., Yan, P., Tang, J., Ma, J., Wang, Z., Gbaguidi, A., and Sun, Y.: Observational study of influence
794 of aerosol hygroscopic growth on scattering coefficient over rural area near Beijing mega-city,
795 *Atmos. Chem. Phys.*, 9, 7519-7530, 2009.

796 Pilinis, C., Seinfeld, J. H., and Grosjean, D.: Water content of atmospheric aerosols, *Atmos. Environ.*, 23,
797 1601-1606, 1989.

798 Pilinis, C., Pandis, S. N., and Seinfeld, J. H.: Sensitivity of direct climate forcing by atmospheric aerosols
799 to aerosol size and composition, *J. Geophys. Res.*, 100, 18739-18754, 1995.

800 Qi, H., Lin, W., Xu, X., Yu, X., and Ma, Q.: Significant downward trend of SO₂ observed from 2005 to
801 2010 at a background station in the Yangtze Delta region, China, *Sci. China Ser. B*, 55, 1451-1458,
802 2012.

803 Quinn, P., Marshall, S., Bates, T., Covert, D., and Kapustin, V.: Comparison of measured and calculated
804 aerosol properties relevant to the direct radiative forcing of tropospheric sulfate aerosol on climate,
805 *J. Geophys. Res.*, 100, 8977-8991, 1995.

806 Quinn, P. K., Bates, T. S., Baynard, T., Clarke, A. D., Onasch, T. B., Wang, W., Rood, M. J., Andrews, E.,
807 Allan, J., Carrico, C. M., Coffman, D., and Worsnop, D.: Impact of particulate organic matter on the
808 relative humidity dependence of light scattering: A simplified parameterization, *Geophys. Res. Lett.*,
809 32, L22809, doi: 10.1029/2005gl024322, 2005.

810 Randles, C., Russell, L., and Ramaswamy, V.: Hygroscopic and optical properties of organic sea salt
811 aerosol and consequences for climate forcing, *Geophys. Res. Lett.*, 31, L16108,
812 doi:10.1029/2004GL020628, 2004.

813 Shen, X., Sun, J., Zhang, Y., Wehner, B., Nowak, A., Tuch, T., Zhang, X., Wang, T., Zhou, H., and Zhang, X.:

814 First long-term study of particle number size distributions and new particle formation events of
815 regional aerosol in the North China Plain, *Atmos. Chem. Phys.*, **11**, 1565-1580,
816 doi:10.5194/acp-11-1565-2011, 2011.

817 Shi, Y., Chen, J., Hu, D., Wang, L., Yang, X., and Wang, X.: Airborne submicron particulate (PM₁)
818 pollution in Shanghai, China: Chemical variability, formation/dissociation of associated
819 semi-volatile components and the impacts on visibility, *Sci. Total Environ.*, **473**, 199-206, 2014.

820 Shi, Z., Zhang, D., Hayashi, M., Ogata, H., Ji, H., and Fujiie, W.: Influences of sulfate and nitrate on the
821 hygroscopic behaviour of coarse dust particles, *Atmos. Environ.*, **42**, 822-827, 2008.

822 Sjogren, S., Gysel, M., Weingartner, E., Baltensperger, U., Cubison, M., Coe, H., Zardini, A., Marcolli, C.,
823 Krieger, U., and Peter, T.: Hygroscopic growth and water uptake kinetics of two-phase aerosol
824 particles consisting of ammonium sulfate, adipic and humic acid mixtures, *J. Aerosol Sci.*, **38**,
825 157-171, 2007.

826 Sullivan, R., Moore, M., Petters, M., Kreidenweis, S., Roberts, G., and Prather, K.: Effect of chemical
827 mixing state on the hygroscopicity and cloud nucleation properties of calcium mineral dust particles,
828 *Atmos. Chem. Phys.*, **9**, 3303-3316, 2009.

829 Sun, J., Zhang, Q., Canagaratna, M. R., Zhang, Y., Ng, N. L., Sun, Y., Jayne, J. T., Zhang, X., Zhang, X., and
830 Worsnop, D. R.: Highly time- and size-resolved characterization of submicron aerosol particles in
831 Beijing using an Aerodyne Aerosol Mass Spectrometer, *Atmos. Environ.*, **44**, 131-140, 2010.

832 Sun, Y., Wang, Z., Dong, H., Yang, T., Li, J., Pan, X., Chen, P., and Jayne, J. T.: Characterization of summer
833 organic and inorganic aerosols in Beijing, China with an Aerosol Chemical Speciation Monitor,
834 *Atmos. Environ.*, **51**, 250-259, 2012.

835 Tang, I. N.: Chemical and size effects of hygroscopic aerosols on light scattering coefficients, *J. Geophys.*
836 *Res.-Atmos.*, **101**, 19245-19250, 1996.

837 Tobo, Y., Zhang, D., Matsuki, A., and Iwasaka, Y.: Asian dust particles converted into aqueous droplets
838 under remote marine atmospheric conditions, *P. Natl. Acad. Sci. USA*, **107**, 17905-17910, 2010.

839 Tuch, T. M., Haudek, A., Müller, T., Nowak, A., Wex, H., and Wiedensohler, A.: Design and performance
840 of an automatic regenerating adsorption aerosol dryer for continuous operation at monitoring sites,
841 *Atmos. Meas. Tech.*, **2**, 417-422, doi:10.5194/amt-2-417-2009, 2009.

842 Wang, Y., Zhang, X., and Draxler, R. R.: TrajStat: GIS-based software that uses various trajectory
843 statistical analysis methods to identify potential sources from long-term air pollution measurement
844 data, *Environ. Modell. Softw.*, **24**, 938-939, 2009.

845 Wang, J. and Martin, S. T.: Satellite characterization of urban aerosols: Importance of including
846 hygroscopicity and mixing state in the retrieval algorithms, *J. Geophys. Res.-Atmos.*, **112**, D17203,
847 doi:10.1029/2006JD008078, 2007.

848 Wang, M. X., Ding, X., Fu, X., He, Q., Wang, S., Bernard, F., Zhao, X., and Wu, D.: Aerosol scattering
849 coefficients and major chemical compositions of fine particles observed at a rural site in the central
850 Pearl River Delta, South China, *J. Environ. Sci.*, **24**, 72-77, 2012.

851 Wang, L. P., Zhang, B. H., and Zhang, X. W.: Main weather processes in March and April, 2013, *Weather*
852 *Forecast Rev.*, **5**, 1-7, 2013.

853 Weingartner, E., Baltensperger, U., and Burtscher, H.: Growth and structural change of combustion
854 aerosols at high relative humidity, *Environ. Sci. Technol.*, **29**, 2982-2986, 1995.

855 Wiscombe, W., and Grams, G.: The backscattered fraction in two-stream approximations, *J. Atmos. Sci.*,
856 **33**, 2440-2451, 1976.

857 Xu, J., Bergin, M., Yu, X., Liu, G., Zhao, J., Carrico, C., and Baumann, K.: Measurement of aerosol

858 chemical, physical and radiative properties in the Yangtze delta region of China, *Atmos. Environ.*, 36,
859 161-173, 2002.

860 Xu, X., Lin, W., Wang, T., Yan, P., Tang, J., Meng, Z., and Wang, Y.: Long-term trend of surface ozone at a
861 regional background station in eastern China 1991–2006: enhanced variability, *Atmos. Chem. Phys.*,
862 8, 2595-2607, doi:10.5194/acp-8-2595-2008, 2008.

863 Yan, P., Zhang, Y. M., Yang, D. Z., Tang, J., Yu, X. L., Cheng, H. B., and Yu, X. M.: The characteristic of
864 aerosol ionic size distributions at Lin'an in summer of 2003, *Acta Meteor. Sin.*, 63, 980–987, 2005.

865 Yan, P., Pan, X., Tang, J., Zhou, X., Zhang, R., and Zeng, L.: Hygroscopic growth of aerosol scattering
866 coefficient: A comparative analysis between urban and suburban sites at winter in Beijing,
867 *Particuology*, 7, 52-60, 2009.

868 Zhang, B. and Sun, J.: Analysis of the March 2013 atmospheric circulation and Weather, *Meteor. Mon.*,
869 39, 794–800, 2013.

870 Zhang, Y. Y., Zuo, L. F., Ren, X. C., and Cui, J.: Research of the aerosol scattering properties based on
871 evaporation duct, *Ship Electron. Eng.*, 32, 12–14, 2012.

872 [Zhejiang Environmental Protection Bureau \(ZEPB\), 1999, Annual Report on the State of the](#)
873 [Environment of Zhejiang Province, Zhejiang Environmental Protection Bureau, Hangzhou, 1999.](#)

874 Zhejiang Environmental Protection Bureau (ZEPB), 2006, Annual Report on the State of the
875 Environment of Zhejiang Province, Zhejiang Environmental Protection Bureau, Hangzhou, 21 pp.,
876 2006.

877 Zhejiang Environmental Protection Bureau (ZEPB), 2012, Annual Report on the State of the
878 Environment of Zhejiang Province, Zhejiang Environmental Protection Bureau, Hangzhou, 29 pp.,
879 2012.

880 [Zhejiang Environmental Protection Bureau \(ZEPB\), 2013, Annual Report on the State of the](#)
881 [Environment of Zhejiang Province, Zhejiang Environmental Protection Bureau, Hangzhou, 33 pp.,](#)
882 [2013.](#)

883 Zieger, P., Fierz-Schmidhauser, R., Gysel, M., Ström, J., Henne, S., Yttri, K. E., Baltensperger, U., and
884 Weingartner, E.: Effects of relative humidity on aerosol light scattering in the Arctic, *Atmos. Chem.*
885 *Phys.*, 10, 3875-3890, doi:10.5194/acp-10-3875-2010, 2010.

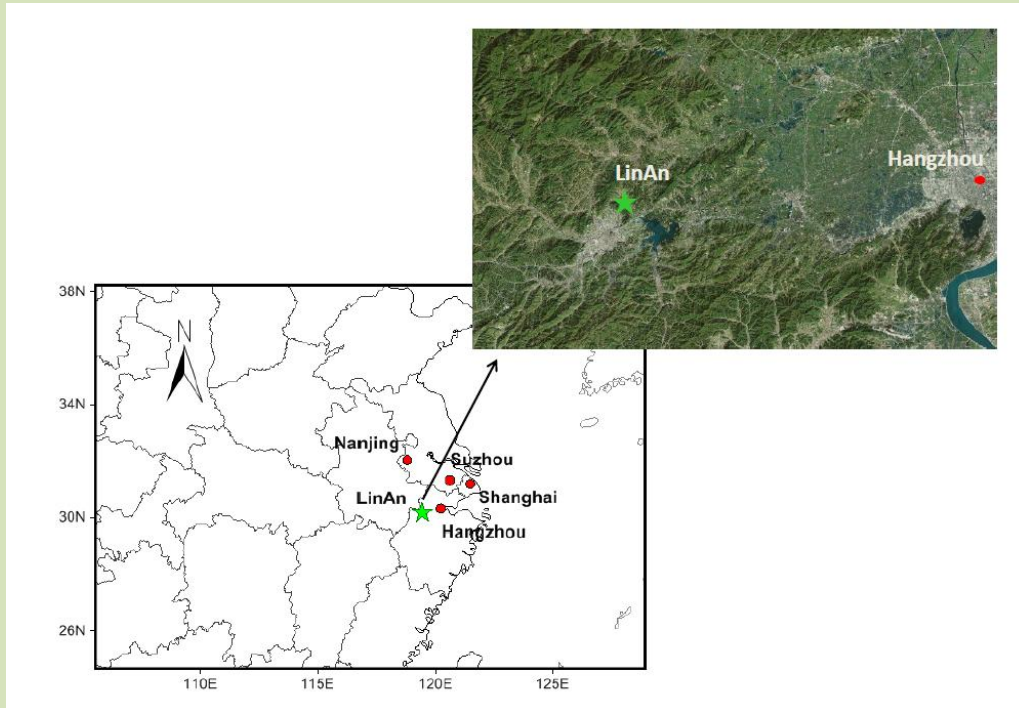
886 Zieger, P., Weingartner, E., Henzing, J., Moerman, M., Leeuw, G. d., Mikkilä, J., Ehn, M., Petäjä, T.,
887 Clémer, K., and Rozendael, M. v.: Comparison of ambient aerosol extinction coefficients obtained
888 from in-situ, MAX-DOAS and LIDAR measurements at Cabauw, *Atmos. Chem. Phys.*, 11, 2603-2624,
889 doi:10.5194/acp-11-2603-2011, 2011.

890 Zieger, P., Kienast-Sjögren, E., Starace, M., Bismarck, J. v., Bukowiecki, N., Baltensperger, U., Wienhold,
891 F., Peter, T., Ruhtz, T., and Collaud Coen, M.: Spatial variation of aerosol optical properties around
892 the high-alpine site Jungfraujoch (3580 m asl), *Atmos. Chem. Phys.*, 12, 7231-7249,
893 doi:10.5194/acp-12-7231-2012, 2012.

894 Zieger, P., Fierz-Schmidhauser, R., Weingartner, E., and Baltensperger, U.: Effects of relative humidity
895 on aerosol light scattering: results from different European sites, *Atmos. Chem. Phys.*, 13,
896 10609-10631, doi:10.5194/acp-13-10609-2013, 2013.

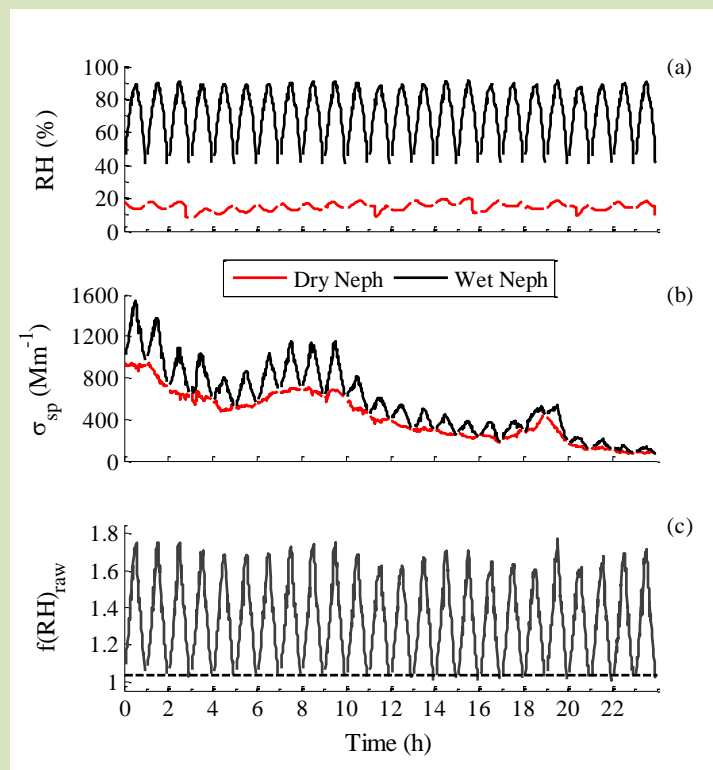
897 Zieger, P., Fierz-Schmidhauser, R., Poulain, L., Müller, T., Birmili, W., Spindler, G., Wiedensohler, A.,
898 Baltensperger, U., and Weingartner, E.: Influence of water uptake on the aerosol particle light
899 scattering coefficients of the Central European aerosol, *Tellus B*, 66, 22716,
900 doi:10.3402/tellusb.v66.22716, 2014.

901



902

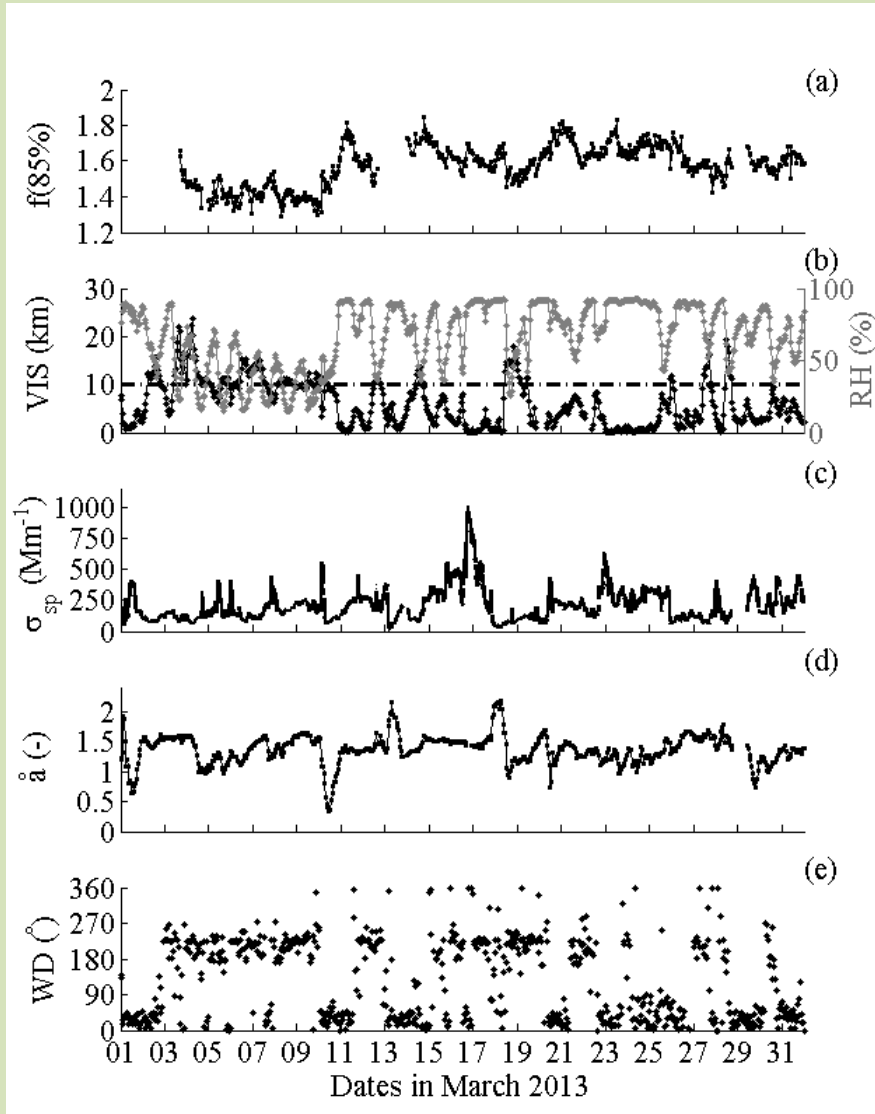
903 Fig. 1 Location of LinAn station (green pentagram) and the main cities in the
 904 Yangtze River Delta (red dots) in the lower left panel. The upper right panel is the
 905 topography of the surrounding area.



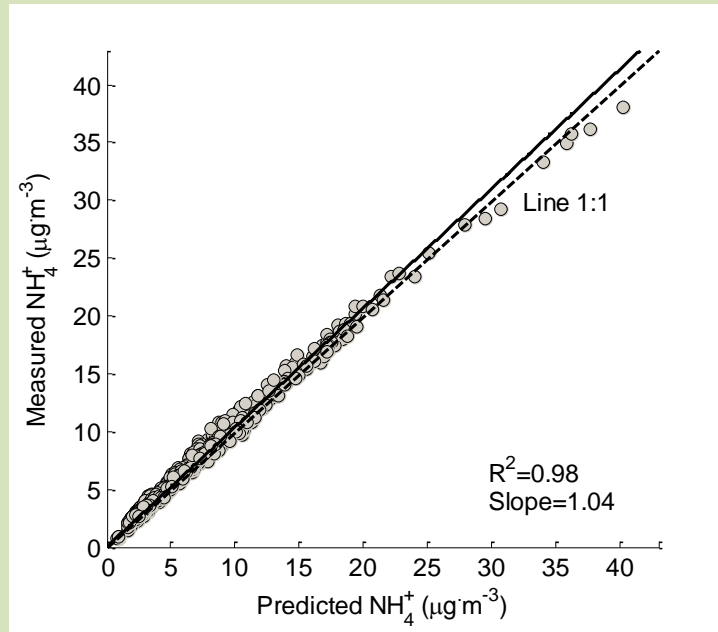
906

907 Fig. 3-2 Example of recorded data on 17 March 2013 (a) Relative humidity of inside
 908 DryNeph (red line) and WetNeph (black line), the black line represents RH=91%; (b)

909 Aerosol scattering coefficients measured by DryNeph (red line) and WetNeph (black
 910 line) at 550nm wavelength; (c) Raw scattering enhancement factor $f(\text{RH}, 550\text{nm})_{\text{raw}}$
 911 without normalization, the black dash line was $f(\text{RH})_{\text{raw}}=1.03$.

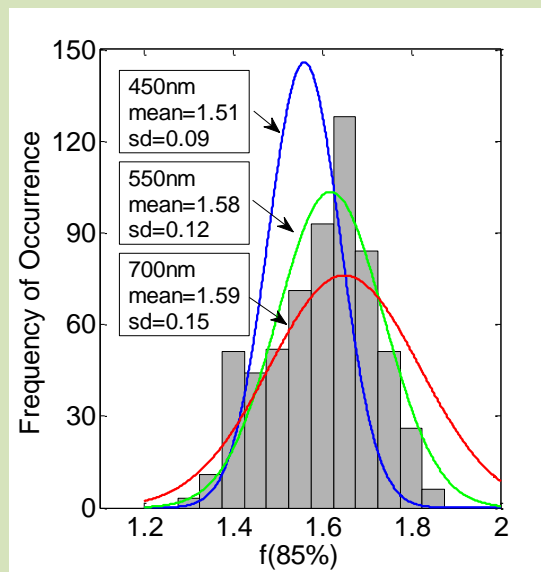


912
 913 Fig. 4-3 Time series of measured and derived aerosol variables, as well as the ambient
 914 RH and visibility. (a) scattering enhancement factor at $\text{RH}=f(85\%)$ at 550 nm
 915 wavelength; (b) visibility (VIS) and relative humidity (RH) at ambient conditions, the
 916 dashed line represents $\text{VIS}=10$ km; (c) aerosol scattering coefficient of DryNeph at
 917 550 nm wavelength; (d) Ångström exponent \tilde{a} (e) wind direction (WD), indicating
 918 prevailing wind directions during observation period was mainly northeasterly (NE)
 919 and southwesterly (SW).



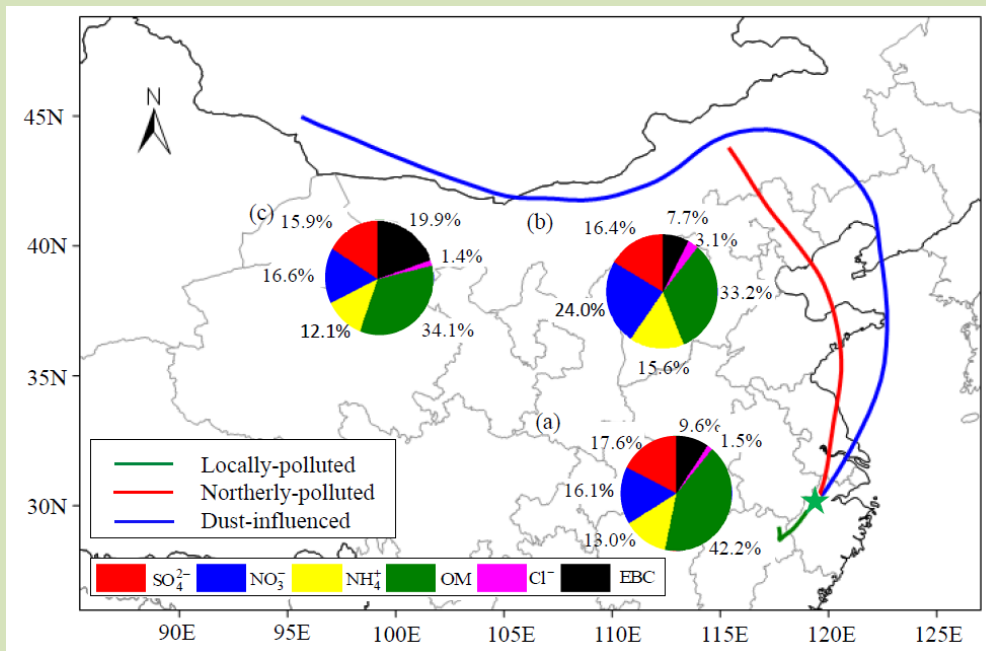
920

921 Fig. 5-4 Measured and predicted mass concentration of ammonium. The predicted
 922 mass concentration of ammonium (NH_4^+ _{predicted}) is calculated by Eq. (4). The solid
 923 black line represents the linear least square regression.



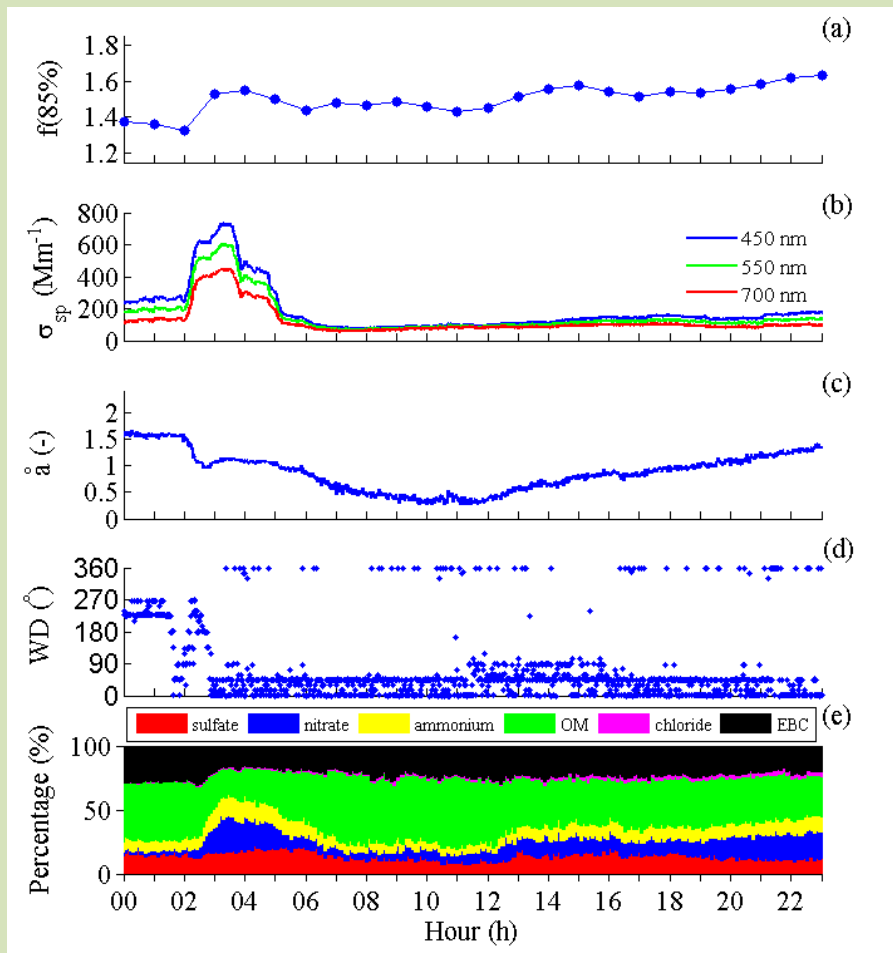
924

925 Fig. 6-5 Histograms of (a) $f(85\%, 550 \text{ nm})$ overlaid with the Gaussian curves based
 926 on the statistics for $f(85\%, 450 \text{ nm})$, $f(85\%, 550 \text{ nm})$ and $f(85\%, 700 \text{ nm})$; (b)
 927 ~~Frequency of occurrence of $f(85\%, 550 \text{ nm})$ - $f(85\%, 450 \text{ nm})$ and (c) $f(85\%, 550$~~
 928 ~~nm) - $f(85\%, 700 \text{ nm})$.~~



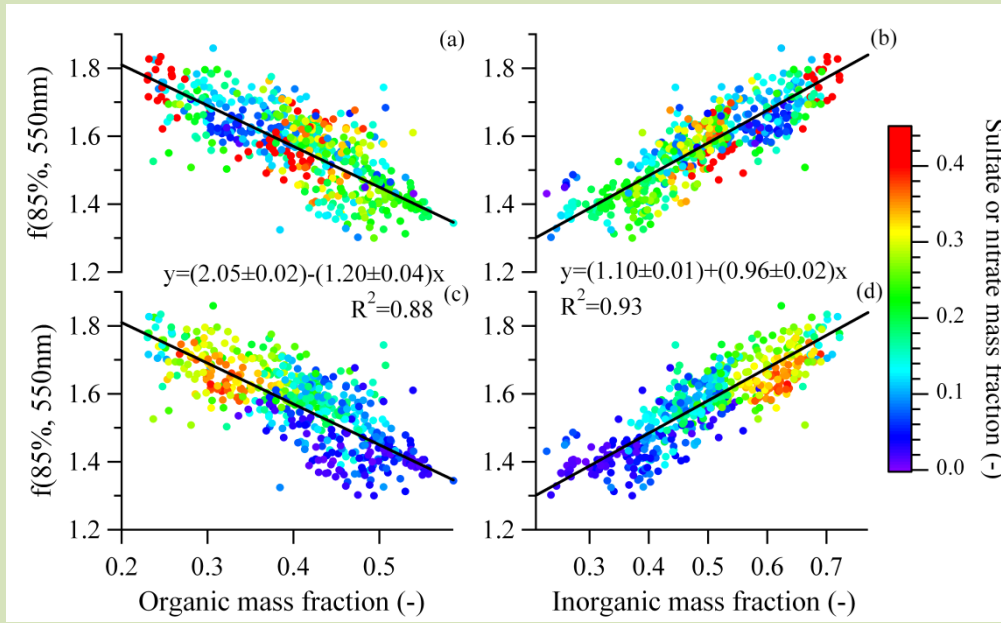
929

930 Fig. 7-6 72h back trajectories of locally-polluted period and
 931 dust-influenced period, together with the mean mass fraction of submicron chemical
 932 compositions (SO_4^{2-} , NO_3^- , NH_4^+ , OM and Cl^-) measured by AMS and EBC in PM_{10}
 933 measured by MAAP. The pie chart (a), (b) and (c) were for locally-polluted,
 934 northerly-polluted and dust-influenced periods, respectively.



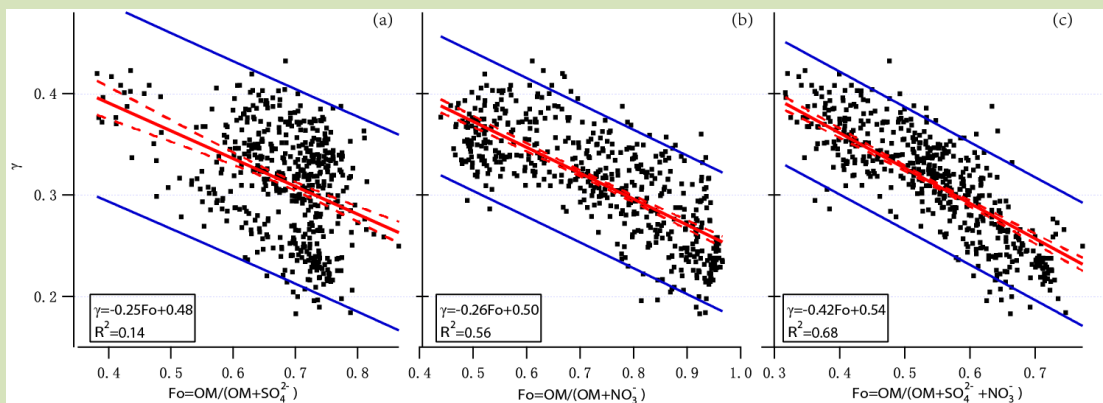
935

936 Fig. 8-7 Parameters in episode influenced by dust on 10 March 2013 at LinAn (a)
 937 scattering enhancement factor at $f(85\%)$ at 550nm wavelength-RH; (b) scattering
 938 coefficients at 450nm, 550nm and 700nm wavelengths; (c) Ångström exponent \hat{a} ; (d)
 939 wind direction; (e) mass percentages of chemical species measured by AMS and
 940 MAAP.



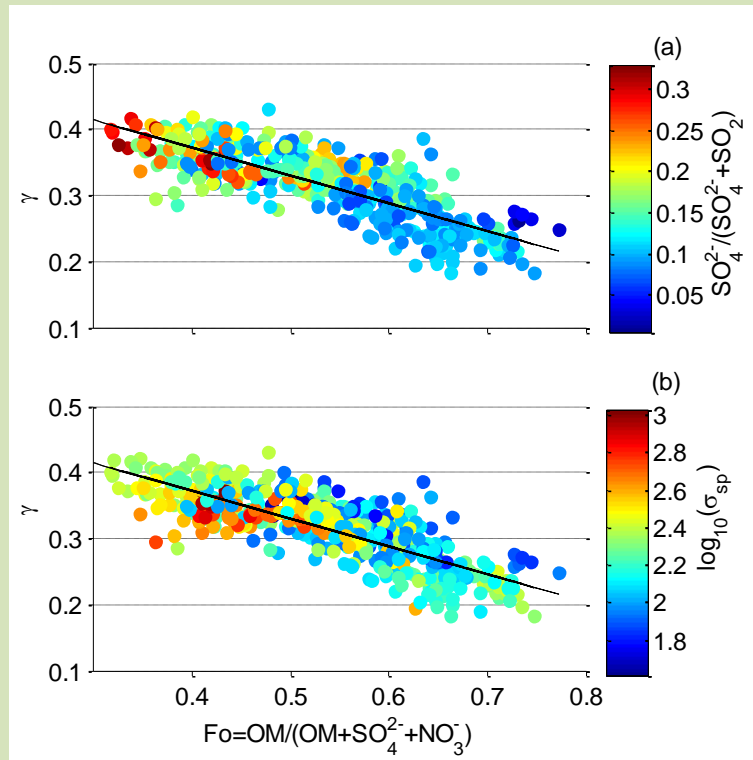
941

942 Fig. 9-8 Scattering enhancement factor $f(85\%, 550\text{nm})$ vs. organic mass fraction and
 943 inorganic mass fraction determined from AMS and MAAP: (a) (b) $f(85\%, 550\text{nm})$ vs.
 944 organic mass and inorganic mass fraction colored by sulfate mass fraction,
 945 respectively; (c) (d) $f(85\%, 550\text{nm})$ vs. organic mass fraction and inorganic mass
 946 fraction colored by nitrate mass fraction, respectively. The Solid-solid black lines
 947 represent the linear least square regression a bivariate linear regression including the
 948 uncertainty of $f(85\%, 550\text{nm})$ and the standard deviation of chemical compositions.



949

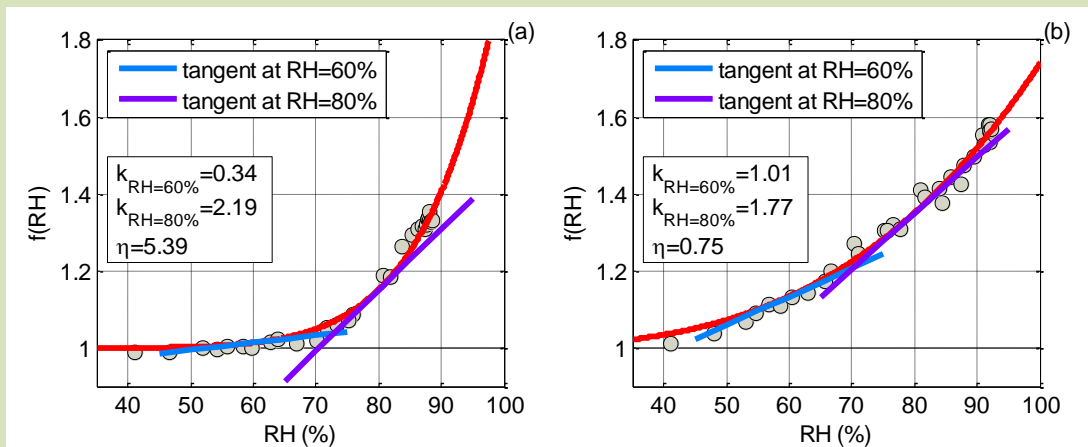
950 Fig. 10-9 scatter plots of γ versus F_o (a) $F_o = \text{OM} / (\text{OM} + \text{SO}_4^{2-})$, (b) $F_o = \text{OM} / (\text{OM} + \text{NO}_3^-)$
 951 and (c) $F_o = \text{OM} / (\text{OM} + \text{SO}_4^{2-} + \text{NO}_3^-)$. Solid red lines represent the linear fit, dashed red
 952 lines show the 95% confidence level for the fit, and solid blue lines show the 95%
 953 prediction bands.



954

955 Fig. 41-10 γ versus $F_o = \text{OM}/(\text{OM} + \text{SO}_4^{2-} + \text{NO}_3^-)$ colored by (a) $\text{SO}_4^{2-}/(\text{SO}_4^{2-} + \text{SO}_2)$

956 molar ratio and (b) $\log_{10}(\sigma_{\text{sp}})$.



957

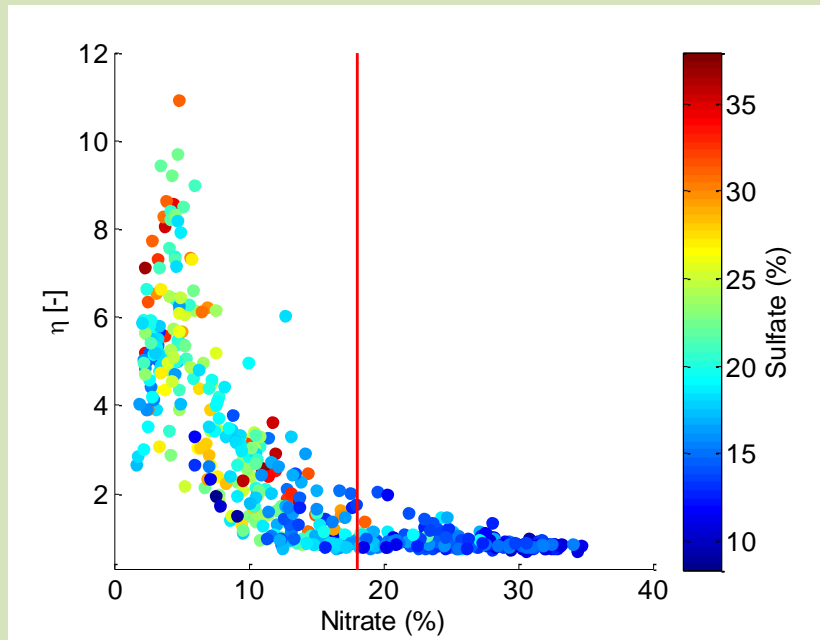
958 Fig. 42-11 Two distinct examples showing different growth patterns and the

959 corresponding η (a) 2013.03.08 18h $f(\text{RH})$ increased slowly at low RH (usually <70%)

960 and then increase more steeply, thus η is big; (b) 2013.03.10 21h $f(\text{RH})$ increased with

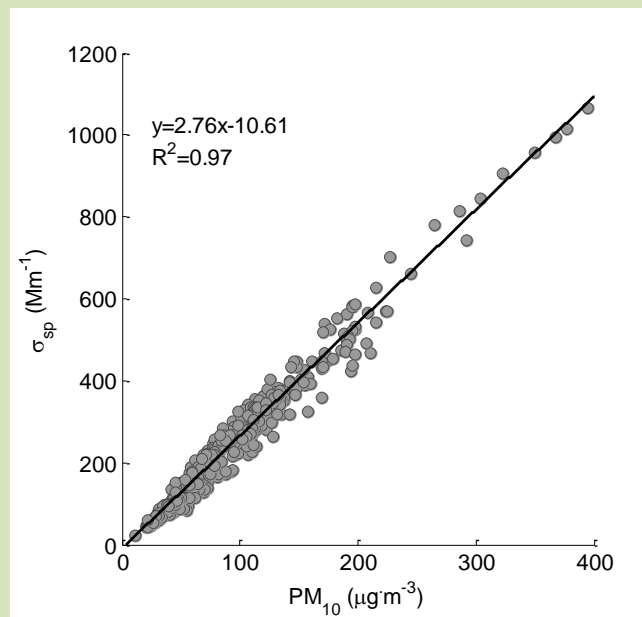
961 nearly constant speed and η is small. $k_{\text{RH}=60\%}$ and $k_{\text{RH}=80\%}$ represent the derivatives at

962 60% and 80% RH, respectively. $f(\text{RH})$ were at 550nm wavelength.



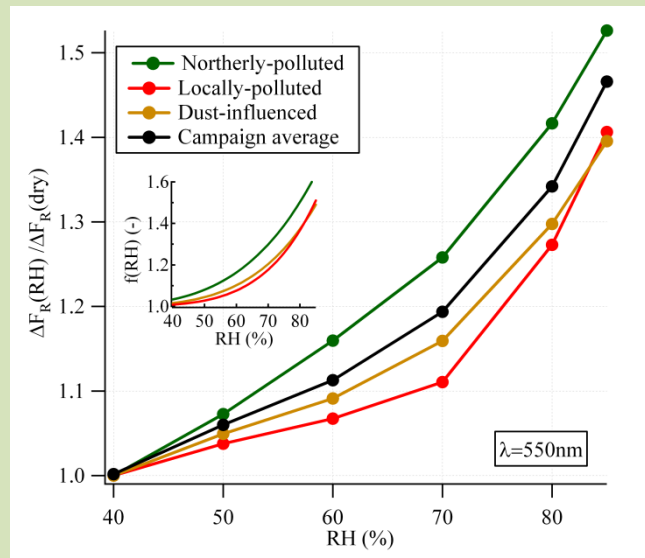
963

964 Fig. 13-12 Scatter plot of η and the mass percentage of nitrate, colored by the mass
 965 percentage of sulfate.



966

967 Fig. 14-13 Linear regression of scattering coefficients (σ_{sp}) at 550nm wavelength and
 968 PM_{10} mass concentration.



969
 970 Fig. 14 Influence of relative humidity (RH) on direct radiative forcing for the entire
 971 campaign (black line), as well as for the northerly-polluted, locally-polluted and
 972 dust-polluted periods, measured by the ratio of radiative forcing at a certain RH to
 973 that at dry conditions. The small inlay shows the fitting curves of $f(RH)$ for
 974 northerly-polluted, locally-polluted and dust-polluted periods, respectively, using
 975 fitting parameters in Table 6. All the parameters were measured at 550nm wavelength.

976
 977 Table 1 Averaged enhancement factors and mean standard deviations for scattering
 978 coefficient, backscattering coefficient and hemispheric backscatter fraction at
 979 different RHs (550nm wavelength).

| RH(%) | $f(RH)$ | $f_b(RH)$ | $f_\beta(RH)$ |
|-------|------------|------------|---------------|
| 50 | 1.07(0.04) | 1.04(0.02) | 0.96(0.02) |
| 60 | 1.14(0.08) | 1.06(0.04) | 0.93(0.04) |
| 70 | 1.24(0.11) | 1.10(0.05) | 0.89(0.05) |
| 80 | 1.43(0.12) | 1.18(0.07) | 0.83(0.05) |
| 85 | 1.58(0.12) | 1.25(0.07) | 0.79(0.04) |

980
 981 Table 2 Summary of mass concentrations ($\mu\text{g}\cdot\text{m}^{-3}$) of aerosol species measured by
 982 AMS as well as MAAP(*) (SD: standard deviation)

| Mean | SD | Minimum | Maximum |
|------|----|---------|---------|
|------|----|---------|---------|

| | | | | |
|----------|------|------|-------|------|
| Sulfate | 8.1 | 4.1 | 0.1 | 26.1 |
| Nitrate | 9.8 | 12.1 | 0.2 | 79.2 |
| Ammonium | 6.9 | 5.5 | 0.5 | 42.8 |
| Chloride | 1.1 | 2.0 | 0.002 | 22.9 |
| OM | 17.7 | 11.1 | 2.8 | 93.9 |
| EBC* | 4.1 | 2.8 | 0.7 | 25.3 |

983 * EBC was measured by MAAP in PM₁₀.

984

985 Table 3 Statistical values of f(85%) at 450 nm, 550 nm and 700 nm wavelengths (SD:
986 standard deviation; prctl: percentile)

| λ | mean | SD | 90th prctl. | 75th prctl. | median | 25th prctl. | 10th prctl. |
|-----------|------|------|-------------|-------------|--------|-------------|-------------|
| 450 nm | 1.51 | 0.09 | 1.63 | 1.58 | 1.53 | 1.47 | 1.39 |
| 550 nm | 1.58 | 0.12 | 1.72 | 1.65 | 1.59 | 1.49 | 1.40 |
| 700 nm | 1.59 | 0.15 | 1.77 | 1.70 | 1.62 | 1.46 | 1.36 |

987

988 Table 4 Average enhancement factors and mean standard deviations for scattering
989 coefficient, backscattering coefficient and hemispheric backscatter fraction in various
990 observation episodes ([550nm wavelength](#)).

| | Locally-polluted | Northerly-polluted | Dust-influenced |
|---------------------------------------|------------------|--------------------|-----------------|
| f(80%) | 1.36(0.11) | 1.50(0.09) | 1.37(0.05) |
| f _b (80%) | 1.15(0.06) | 1.21(0.06) | 1.15(0.03) |
| f _{β} (80%) | 0.85(0.04) | 0.81(0.03) | 0.84(0.03) |
| f(85%) | 1.52(0.10) | 1.64(0.09) | 1.48(0.05) |
| f _b (85%) | 1.21(0.06) | 1.28(0.06) | 1.19(0.04) |
| f _{β} (85%) | 0.80(0.02) | 0.78(0.02) | 0.81(0.03) |
| N | 295 | 303 | 14 |

991

992 Table 5 Curve-fitting parameters [of f\(RH\) at 550nm wavelength](#) for various aerosol
993 types in terms of equation $f(RH)=c(1-RH)^{-g}$.

| c | g | Reference |
|---|---|-----------|
|---|---|-----------|

| | | | |
|----------------------------|-----------|-----------|-----------------------|
| Locally-polluted | 0.85±0.08 | 0.29±0.04 | |
| Northerly-polluted | 0.93±0.07 | 0.28±0.03 | This work |
| Dust-influenced | 0.87±0.05 | 0.27±0.02 | |
| Continental | 0.9±0.1 | - | Zieger et al. (2014) |
| Arctic ^a | 1 | 0.58±0.09 | Zieger et al. (2010) |
| Marine | 0.99 | 0.54 | |
| Polluted | 0.59 | 0.77 | Carrico et al. (2003) |
| Dust | 0.60 | 0.61 | |
| Polluted Marine | 1 | 0.57±0.06 | |
| Dust | 1 | 0.23±0.05 | Gass ó et al. (2000) |
| Clean Marine1 ^b | 1 | 0.69±0.06 | |
| Clean Marine2 ^c | 1 | 0.73±0.07 | |

994 a fitting results for aerosol samples with RH>75%

995 b fitting results for aerosol samples with RH>60%

996 c fitting results for aerosol samples with RH>80%

997

998 Table 6 Curve-fitting parameters of f(RH) at 550nm wavelength for various aerosol
 999 types in terms of Eq. (5).

| | a | b | Reference |
|--------------------|-----------|-----------|-------------------|
| Locally-polluted | 1.24±0.29 | 5.46±1.90 | |
| Northerly-polluted | 1.20±0.21 | 3.90±1.27 | This work |
| Dust-influenced | 1.02±0.19 | 4.51±0.80 | |
| Clean | 1.20±0.06 | 6.07±0.27 | |
| Polluted | 2.30±0.03 | 6.27±0.10 | Pan et al. (2009) |
| Dust | 0.64±0.04 | 5.17±0.40 | |
| Urban | 2.06 | 3.60 | |
| Mixed | 3.26 | 3.85 | Liu et al. (2007) |
| Marine | 4.92 | 5.04 | |

1001 Table 7 Estimated effects of aerosol hygroscopic growth on direct radiative forcing by
 1002 locally-polluted, northerly-polluted and dust-influenced aerosols at LinAn, measured
 1003 by the ratio ($\Delta F_R(\text{RH}_{\text{amb}})/\Delta F_R(\text{dry})$) of direct aerosol radiative forcing at the ambient
 1004 average relative humidity ($\text{RH}_{\text{amb}}=67\%$) for the entire campaign to that in dry
 1005 condition. All the parameters were measured at 550nm wavelength.

| | $f(\text{RH}_{\text{amb}})$ | $b(\text{dry})$ | $\bar{\beta}(\text{dry})$ | $b(\text{RH}_{\text{amb}})$ | $\bar{\beta}(\text{RH}_{\text{amb}})$ | $\Delta F_R(\text{RH}_{\text{amb}})/\Delta F_R(\text{dry})$ |
|--------------------|-----------------------------|-----------------|---------------------------|-----------------------------|---------------------------------------|---|
| Entire campaign | 1.21 | 0.126 | 0.268 | 0.115 | 0.255 | 1.157 |
| Locally-polluted | 1.17 | 0.131 | 0.274 | 0.123 | 0.263 | 1.118 |
| Northerly-polluted | 1.26 | 0.121 | 0.262 | 0.106 | 0.243 | 1.195 |
| Dust-influenced | 1.15 | 0.146 | 0.289 | 0.132 | 0.274 | 1.105 |

1006